Rare Met. (2024) 43(9):4076–4098
https://doi.org/10.1007/s12598-024-02808-4

RARE METALS

MINI REVIEW

Mechanism research progress on transition metal compound electrode materials for supercapacitors

Zhi-Hui Xu, Xue-Lei Li, Qing-Wen Li, Kai Lv, Jing-Shun Liu, Xiu-Kun Hang, Aruuhan Bayaguud*

Received: 8 January 2024 / Revised: 29 February 2024 / Accepted: 29 February 2024 / Published online: 30 May 2024

Abstract Supercapacitors (SCs) have remarkable energy storage capabilities and have garnered considerable interest due to their superior power densities and ultra-long cycling characteristics. However, their comparatively low energy density limits their extensive application in large-scale commercial applications. Electrode materials directly affect the performance of SCs. Thus, the development of cutting-edge electrode materials and modification of their morphological and structural properties are vital for advancing the performance of SCs. Transition metal compounds have a high specific capacity and good cycling durability, making them the most promising electrode active materials for high-energy density SCs. Nevertheless, their inadequate conductivity, unfavorable ion diffusion rates, substantial volume expansion and phase transitions during charging and discharging are obstacles to their stable and efficient integration into SCs. To address these challenges, this study provides a comprehensive summary of the current advancements in transition metal nanomaterials as electrode materials for SCs, an overview of the current research status, and the prevailing challenges. Furthermore, this study highlights synthetic techniques and management strategies for electrode materials derived from transition metal compounds, targeting the resolution of the aforementioned challenges. Finally, a concise discussion is provided on the future directions of SC development, with an emphasis on the utilization of transition metal compound electrode materials.

Keywords Supercapacitors; Transition metal compounds electrode; Existing problems; Synthetic methods; Regulation strategies

1 Introduction

Energy storage has emerged as a significant research area in recent years. The growing demand for fossil fuels exacerbates the depletion of nonrenewable resources and causes environmental pollution and increasingly frequent natural disasters, imposing severe impacts on human health and ecosystems [1, 2]. Therefore, there is an urgent demand for clean and sustainable energy supply technologies, which have continuously stimulated research and investment in many cutting-edge technologies in related fields worldwide [3–6]. Supercapacitors (SCs) offer notable energy storage benefits compared to traditional capacitors. However, they exhibit a maximum energy density that is markedly lower than that of rechargeable secondary batteries [7]. SCs can achieve rapid charge–discharge within seconds to minutes, it takes minutes to several hours for secondary batteries to complete the charge–discharge process [8]. In addition, SCs have advantages such as long cycle stability, high-power density, high safety factor, high energy conversion efficiency, good ultralow-temperature characteristics, convenient detection and environmentally friendly production [9–11].

Z.-H. Xu, X.-L. Li, Q.-W. Li, K. Lv, J.-S. Liu, A. Bayaguud*
School of Materials Science and Engineering, Inner Mongolia University of Technology, Hohhot 010051, China
e-mail: jinaruhan@imut.edu.cn

Z.-H. Xu
School of Materials Science and Engineering, Tianjin University of Technology, Tianjin 300384, China

X.-K. Hang
College of Chemistry and Chemical Engineering, Inner Mongolia University, Hohhot 010021, China

Generally, SCs were only classified according to the nature of material: carbon-based and metal-based materials. These materials are well-categorized accordingly into their storage mechanism: electrochemical double layer capacitors (EDLCs) and pseudocapacitors (PCs), respectively. EDLCs were first introduced by Helmholtz et al. based on the electric double layer theory, which indicated that energy storage in EDLCs was facilitated by the creation of a double electric layer at the interface between the electrolyte and various electrode materials, including activated carbon, carbon fibers and graphene [12]. During charging, the positive and negative charges on the electrode, under the influence of an electric field, draw anions and cations present in the electrolyte, respectively. After reaching the surfaces of the positive and negative electrodes, the electrolyte ions are transferred onto the electrode material surface via Coulomb, Van der Waals and other forces. At the same time, opposite charges appear on the electrode and a stable double layer exists at the interface between the electrode material and the electrolyte, completing electric energy storage. During the operation of EDLCs, anions and cations in the electrolyte undergo only electromigration and diffusion, which are physical phenomena that do not occur during the electrochemical reaction with the electrode. PCs mainly utilize the fast reversible redox reactions of metal oxides to achieve charge storage and release. The theory of pseudocapacitance was first proposed by Conway [13] based on the concept of underpotential deposition involving electroactive substances. This process occurs either on the electrode surface or within the two-dimensional (2D) or quasi-2D spaces of the bulk phase. Subsequently, the capacitance associated with the charging potential of the electrode arises from highly reversible chemical processes, specifically, adsorption/desorption or redox reactions. The charge–discharge reaction process is as follows: $MO_{x\text{-}1} + H^+ - e^- \leftrightarrow MO_{x\text{-}1}(OH)$ (acidic conditions); $MO_x + OH - e^- \leftrightarrow MO_x(OH)$ (alkaline conditions) [14, 15]. Generally, energy storage methods for PCs include double layer energy storage and charge storage, in which the active materials in the electrode react chemically. PCs exhibit greater capacitance and energy density than EDLCs due to the occurrence of redox reactions within the material, not limited to their surfaces.

However, with the rapid development of nanoscience and nanotechnology in recent years, nanomaterial-based electrodes are playing increasingly important roles in electrochemical energy storage. Nanomaterials are small with large surface areas, meaning that their "surface" and "bulk" cannot be clearly distinguished. Accordingly, some Faradaic electrode materials that typically show strong redox reactions in bulk exhibit behaviors such as pseudocapacitance when reduced in size to the nanoscale, characteristic of the disappearance of the redox peaks in cyclic voltammetry (CV) and plateaus in galvanostatic charge–discharge (GCD) curves. An increasing number of studies have demonstrated that crystal phase, surface or interfacial effects may introduce pseudocapacitive contribution in the charge storage process of battery electrodes. Consequently, the boundary between battery and pseudocapacitive materials has blurred in recent years. Terms such as "intercalation pseudocapacitance" and "extrinsic pseudocapacitance" as well as kinetic analysis toward CV have been proposed to better understand the charge storage mechanisms of emerging electrode materials. Indeed, these definitions and methods help distinguish between batteries and pseudocapacitive materials; however, many researchers misunderstand or misuse them, reducing their utility in the electrochemistry community. To accurately distinguish between pseudocapacitive and battery materials, a method was proposed that considered both the electrochemical signatures (CV and GCD) and quantitative kinetics analysis as a supplement (calculation of b in formula $i(V) = av^b$). EDLC materials have a rectangular CV curve, a potential of GCD linear with respect to time, and a value of b always equal to 1. In contrast, pseudocapacitive materials have an approximately rectangular CV and a GCD curve with an almost linear relationship between potential and time. In addition, compared with EDLC, there should be some inflection points in the GCD curve but no obvious plateaus. The calculated b-value is close to 1. For battery-type materials, the typical CV has obvious redox peaks and the GCD shows detectable plateaus (regardless of whether the peaks/plateaus disappear at high rates). The b value should be 0.5, which is generally obtained in traditional bulk battery electrode materials; however, for nanomaterial battery electrodes or those with specific electrode engineering and structural design, the b value may be > 0.5, provided that the redox process is no longer limited by ion diffusion. Researchers have demonstrated differences among symmetric, asymmetric and hybrid devices based on the three electrode materials (EDLC, pseudocapacitive and battery). Symmetric devices use identical materials as the positive and negative electrodes, such as EDLC-type AC//EDLC-type AC, battery-type $Ni(OH)_2$//battery-type $Ni(OH)_2$ or pseudocapacitive-type MnO_2//pseudocapacitive-type MnO_2. Asymmetric devices include EDLC and/or pseudocapacitive electrodes of two different materials. The configuration of asymmetric devices can be classified as pseudocapacitive-type Nb_2O_5//EDCL-type AC, pseudocapacitive-type Nb_2O_5//pseudocapacitive-type MnO_2 or EDLC-type AC//EDCL-type carbon nanotube (CNT). Hybrid devices combine the advantages of EDLC, batteries and pseudocapacitive materials. The hybrid device configuration can be battery-type $Ni(OH)_2$//EDCL-type AC or battery-type $Ni(OH)_2$//pseudocapacitive-type Nb_2O_5.

Combining these advantages improves the specific capacitance cycle stability, and energy density of the material and broadens the working voltage range. The large capacity, high-power charge and discharge of SCs are derived from these two principles, according to which high-performance SCs can be prepared.

Among the components of a SC, the electrode material is of paramount significance for effective charge storage. The electrode material must exhibit good chemical stability. Otherwise, the performance of the SCs is diminished. At the same time, ions and electrons are required to have good electrical conductivity. Only when the electrode materials meet the above requirements, SCs can exhibit good performance and better application [16–19]. Therefore, the advancement of electrode materials with superior performance has emerged as a crucial factor in enhancing the efficiency of SCs and represents the most direct avenue to achieve their practical implementation. Currently, the electrode materials of SCs predominantly involve carbon-based materials, conductive polymers, metal compounds and MXenes, as proposed by Gogotsi et al. [20–24]. In the context of SCs, metal compounds serve as electrode materials, offering higher energy density than carbon materials, and exhibit superior electrochemical stability compared to conductive polymers [25]. Metal compounds can be divided into single- and multi-metallic compounds based on the number of metal atoms. Single-metal compounds have been studied as electrode materials, including Mn-based single-metal compounds [26], Co-based single-metal compounds [27] and Ni-based monometallic compounds [28]. To compensate for the shortcomings of various single-metal compounds and fully exploit the advantages of various metal-atom electrochemical performances, researchers have found that metal ternary materials exhibit better conductivities and cycle performances than binary materials. To date, multimetal compounds have been applied as active electrode materials for energy storage devices and have achieved excellent electrochemical performance [29–32]. Currently, multimetal oxides and hydroxides [33, 34] are the main metal compounds used as electrode materials for SCs, and a small number of multimetal sulfides [35] and phosphides [36, 37] have been reported (Fig. 1).

In this paper, the research status and existing issues of transition metal compound electrode materials for SCs are comprehensively reviewed. Moreover, we focus on the synthetic methods and regulation strategies of transition metal compound electrode materials to address these issues. Finally, we discuss the future development directions of transition metal compound electrode materials for SCs.

2 Research status and existing problems

To attain remarkable performance in SCs, extensive research has been conducted on a variety of metal compounds, including transition metal oxides/hydroxides, transition metal sulfides, transition metal phosphides and transition metal selenides [38–40]. However, there are still great challenges in ensuring their stable and efficient use in SCs to their disadvantages.

2.1 Transition metal oxide/hydroxide

Transition metal oxides/hydroxides have the advantages of high specific capacitance, high conductivity, vast natural abundance, rich valence states and easy design and manufacture [41]. To date, extensive research efforts have been dedicated to investigating a wide range of metal oxides/hydroxides, including RuO_2 [42], MnO_2 [26], NiO [43], SnO_2 [44], Co_3O_4 [45], $Ni(OH)_2$ [46] and $Co(OH)_2$ [47]. In particular, RuO_2 is one of the most classical pseudocapacitance (PC) materials due to its exceptional theoretical specific capacitance (1450 $F{\cdot}g^{-1}$), excellent electrochemical reversibility, high proton conductivity and high rate performance. In addition, RuO_2 has a wide potential window and abundant valence states [48, 49]. When the RuO_2 electrode is charged in an alkaline solution, three oxidation states (RuO_4^{2-}, RuO^{4-} and RuO_4) are formed. These high-valence intermediates are completely reduced to the initial valence state during the discharge process, thus facilitating Faraday charge transfer. Jow et al. believed that the energy storage process of RuO_2 mainly involved the following reactions [49]:

$$RuO_2 + xH^+ + xe^- \leftrightarrow RuO_{2-x}(OH)_x (0 \le x \le 2) \quad (1)$$

Kim et al. successfully synthesized carbon nanofibres with RuO_2 electrode materials loaded on the surface using precipitation and recrystallization (Fig. 2a, b), which exhibited a wide voltage range of − 0.2–0.8 V in 6 $mol{\cdot}L^{-1}$ KOH electrolyte (Fig. 2c) and specific capacitance of 188 $F{\cdot}g^{-1}$ at 1 $mA{\cdot}cm^{-2}$ (Fig. 2d) [50]. Although RuO_2 has excellent electrochemical properties, its poor long-term cycle performance and high manufacturing costs hinder its application.

MnO_2 is another classic PC material after RuO_2 and is a base metal oxide with good electrochemical performance in neutral environments (Na_2SO_4 and K_2SO_4). Notably, MnO_2 exhibits high theoretical capacitance (1390 $F{\cdot}g^{-1}$), cost-effectiveness, minimal toxicity and environmentally friendly attributes. Researchers have extensively investigated its properties and harnessed its potential for various applications [51]. The MnO_2 electrode has good pseudocapacitance characteristics owing to the changes in various Mn valence states ($Mn^{2+}/Mn^{3+}/Mn^{4+}Mn^{5+}$) during

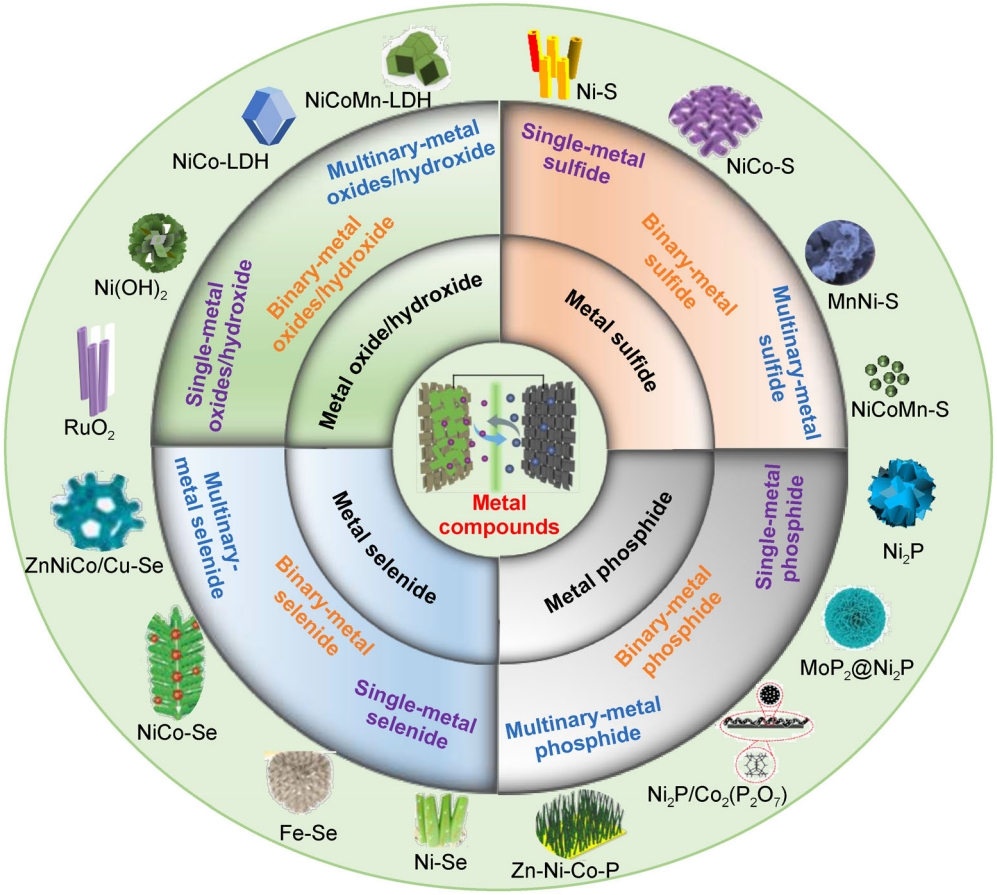

Fig. 1 Schematic diagram of transition metal oxide/hydroxide, sulfide, phosphide and selenide

charging and discharging. Cheng et al. [52] suggested that MnO_2 may be involved in the following reversible energy storage processes:

$$MnO_2 + H^+ + e^- \leftrightarrow MnOOH \quad (2)$$

$$MnO_2 + M^+ + e^- \leftrightarrow MnOOH \quad (3)$$

$$2MnOOH \leftrightarrow Mn^{2+} + MnO_2 + 2OH- \quad (4)$$

where M is an alkali metal ion (Na^+ or K^+). For example, Xu et al. [53] fabricated an ultrafine electrode composed of MnO_2 nanowires grown on carbon cloth (CC) without binders using a simple hydrothermal technique. The ultrafine MnO_2 nanowires developed on the CC exhibited a weed-like morphology, forming a complex and interconnected network (Fig. 2e, f). The distinctive pore structure facilitates the formation of a substantial surface area at the interfaces, allowing the rapid diffusion of electrolytes and efficient electron transfer. The material displayed a remarkable specific capacitance (1174.3 $F{\cdot}g^{-1}$ at 2 $A{\cdot}g^{-1}$), exceptional rate performance and impressive cycling stability (Fig. 2g, h). Nevertheless, their application in SCs faces significant limitations owing to their inadequate conductivity and sluggish ion transfer rates [26].

In addition, CoO and Co_3O_4, well-regarded metal oxides, have become focal points in SC research due to their ability to adapt to various structural configurations, impressive theoretical specific capacitance (3560 $F{\cdot}g^{-1}$), and chemical stability [54]. Cheng et al. suggested that CoO may be involved in the following reversible reactions in the energy storage process [27]:

$$CoO + OH^- \leftrightarrow CoOOH + e^- \quad (5)$$

$$CoOOH + OH^- \leftrightarrow CoO_2 + H_2O + e^- \quad (6)$$

$$CoOOH + H_2O + e^- \leftrightarrow Co(OH)_2 + OH^- \quad (7)$$

For example, Xiao et al. [55] successfully synthesized one-dimensional (1D) CoO nanobelts and 2D CoO nanoplates with porous structures. These materials were obtained by the calcination of single-crystal cobalt hydroxide nanobelts and nanoplates using a solvothermal approach (Fig. 2i, j). The porous CoO nanobelts exhibit a high specific capacitance of 1178 $F{\cdot}g^{-1}$ at 1 $A{\cdot}g^{-1}$. Although Co_3O_4 material has an excellent theoretical specific capacitance, the actual electrode test results are often less than 1,000 $F{\cdot}g^{-1}$ (Fig. 2k). This is due to that the inherent problems of low conductivity, small specific

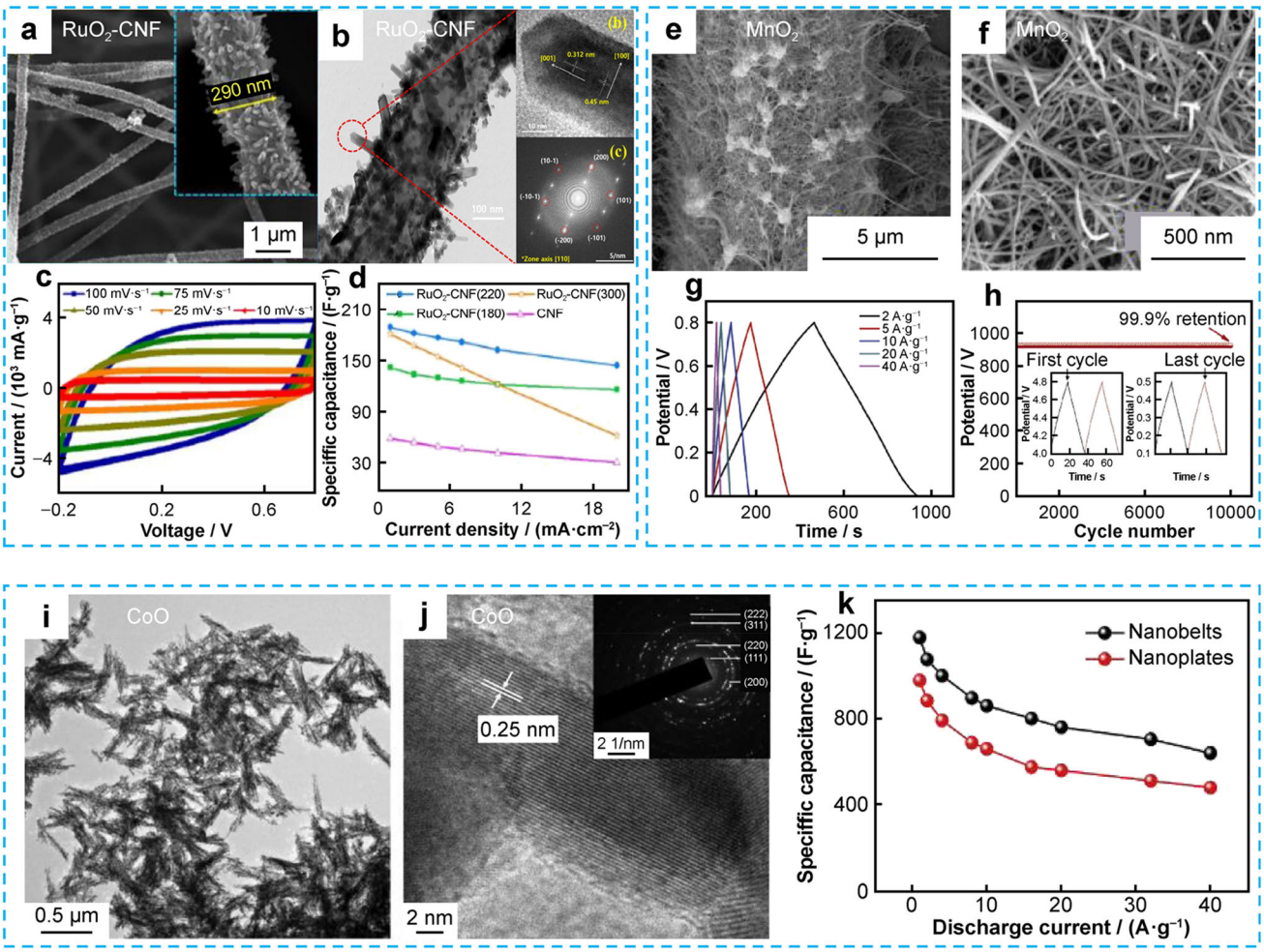

Fig. 2 Characterization and electrochemical performance of RuO_2–CNF nanorods and ultrafine MnO_2 nanowires@CC electrode. **a** SEM, **b** TEM, **c** CV curves and **d** rate performance of RuO_2–CNF nanorods. Reproduced with permission from Ref. [50]. Copyright 2020, ACS Publications. **e**, **f** SEM images, **g** GCD curves and **h** cycle retention of ultrafine MnO_2 nanowires@CC electrode. Reproduced with permission from Ref. [53]. Copyright 2018, Elsevier. **i** TEM and **j** HRTEM images and **k** rate performance curves of CoO nanomaterials. Reproduced with permission from Ref. [55]. Copyright 2019, Elsevier

surface area, slow dynamic process and volume expansion/contraction of the powdered Co_3O_4 material in electrochemical tests seriously limit its specific capacitance and cycle stability [56].

$Ni(OH)_2$-based electrodes have advantages such as outstanding theoretical capacity, strong chemical stability, prominent rate performance, low cost, definite redox transitions and environmental friendliness. In recent years, the synthesis of such electrode materials has increased sharply. Typically, $Ni(OH)_2$ exhibits a hexagonal-layered structure and can exist in two different pseudopolymorphs referred to as the α and β phases. The distinct phases were first described by Bode et al. [57] in 1966. The hydrotalcite-like structured α-$Ni(OH)_2$ is composed of multiple layers of positively charged $Ni(OH)_2$. These layers are enriched with anions such as carbonate, nitrate, chloride, sulfonate and water molecules, resulting in the expansion of the spacing between the layers to 0.72 nm. This arrangement contributes to its superior electrochemical activity compared to β-$Ni(OH)_2$. Additionally, the oxidation state of Ni in α-$Ni(OH)_2$ is + 4, its average oxidation state is 3.3–3.7, which exhibits excellent electrochemical properties compared with β-$Ni(OH)_2$. Lokhande et al. [58] prepared ultrathin α-$Ni(OH)_2$ nanosheets by adding nonionic surfactant Triton X-100 through a simple chemical deposition method. A three-dimensional (3D) mesoporous Ni foam was used as the substrate. The thin nanosheets are skillfully interconnected, creating a unique flower-like structure with pores. This intricate structure played a crucial role in enabling the electrolytes to easily enter the active substance and diminish the diffusion resistance (Fig. 3a, b), resulting in a high specific capacitance of 539 $F \cdot g^{-1}$ at 10 $mV \cdot s^{-1}$ (Fig. 3c, d). It is important to highlight that the metastable phase of α-$Ni(OH)_2$ can rapidly transition into

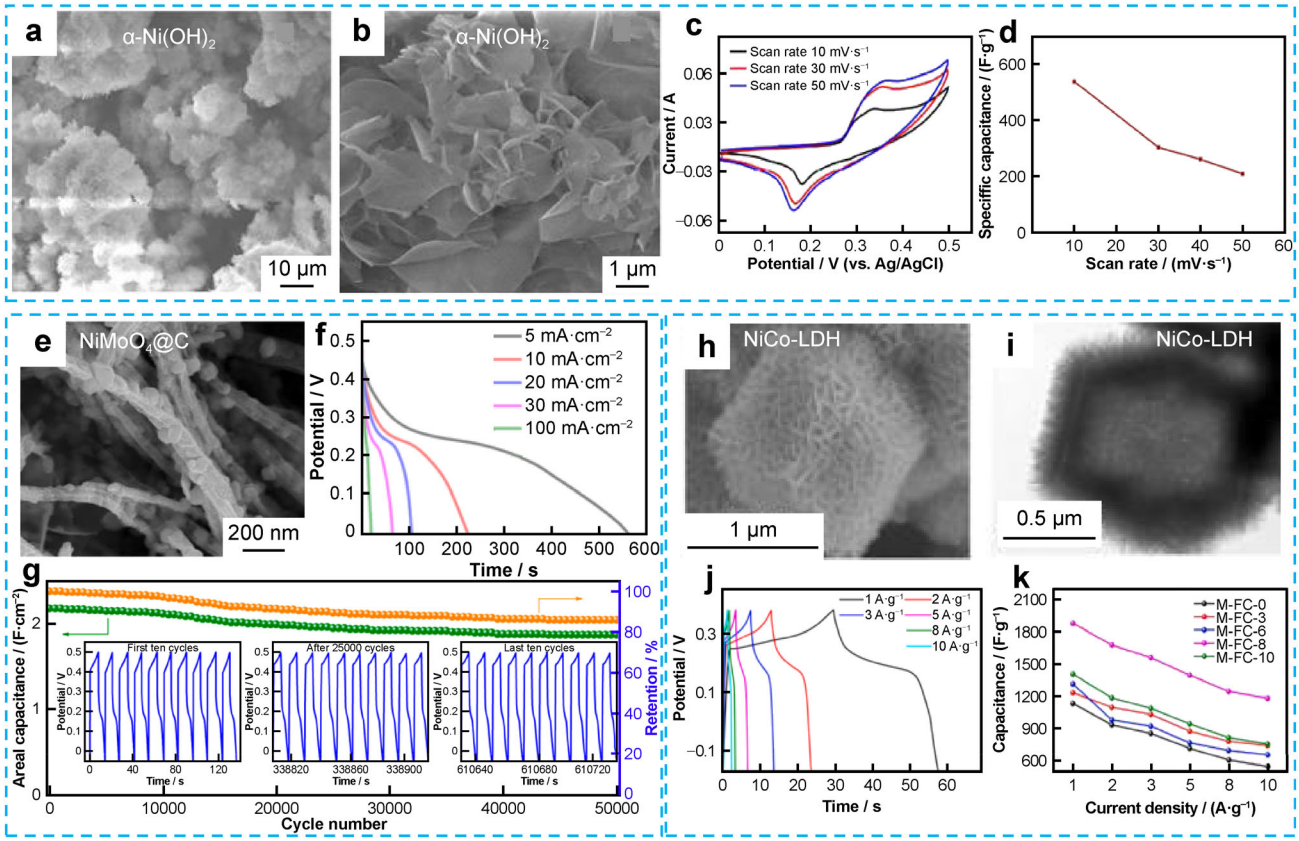

Fig. 3 **a**, **b** SEM images, **c** CV and **d** rate performance curves of α-$Ni(OH)_2$ nanosheets deposited on Ni foam. Reproduced with permission from Ref. [58]. Copyright 2018, Elsevier. Characterization and electrochemical performance of electrode materials. **e** SEM image, **f** GCD curves and **g** cycling stability of $NiMoO_4$@C nanowires. Reproduced with permission from Ref. [66]. Copyright 2017, ACS Publications. **h** SEM and **i** TEM images of NiCo–LDHs; **j** GCD and **k** rate performance curves of NiCo–LDHs. Reproduced with permission from Ref. [63]. Copyright 2023, Elsevier

β-$Ni(OH)_2$ during synthesis and charge–discharge at low discharge current densities. This transformation significantly affects the capacity of SCs, leading to a considerable loss in capacity and a decline in overall cycle performance.

Binary transition metal oxide/hydroxide electrode materials, such as $NiCo_2O_4$ [59], $MnCo_2O_4$ [60], $ZnFe_2O_4$ [61], $MnMoO_4$ [62] and NiCo-hydroxides [63], have attracted research attention. The two metal components of binary transition metal oxide/hydroxide electrode materials undergo redox reactions and contribute to their specific capacitance; thus, binary materials have a higher specific capacitance than single-metal oxides. More importantly, the conductivity of binary metal oxide electrode materials is several times or even dozens of times those of single-metal oxides, thus improving their electronic transmission and cycling performance compared to single-metal materials [64, 65]. Wang et al. [66] prepared a freestanding carbon-coated $NiMoO_4$ nanowire electrode on Ni foam for use in SCs (Fig. 3e). The carbon-coated $NiMoO_4$ nanowire electrode showed a high areal capacitance and remarkable stability during cycling (Fig. 3f, g)). Wang et al. [63] introduced a novel hollow NiCo–LDH electrode through straightforward morphological manipulation (Fig. 3h, i). After optimization, the NiCo–LDH/M–FC electrode demonstrated exceptional specific capacitance and impressive rate performance (Fig. 3j, k). However, its disadvantages are evident in practical applications, such as a short cycle life and a large gap between the actual capacitance and theoretical capacitance.

2.2 Transition metal sulfide

Transition metal sulfides have been widely investigated as a new type of PC material due to their good conductivity, low cost, low electronegativity, good semiconductivity and good redox activity. As the electronegativity of sulfur atoms is weaker than that of oxygen atoms, transition metal sulfides exhibit higher conductivity, thermal stability, mechanical stability and electrochemical performance than their corresponding metal oxides under the same conditions [67, 68]. Nickel sulfide has been explored as an electrode material for SCs due to its abundant phases (e.g., NiS, NiS_2

and Ni_3S_4) and morphological characteristics [69]. Wu et al. [70] introduced an innovative "inner-outer synergistic strategy" for the development of advanced electrode materials. This strategy involves the integration of NiS nanoflakes within electrospun carbon fibers that incorporate NiS nanoparticles (NPs), resulting in a composite material referred to as NiS_{NF}/CF@NiS_{NP} (Fig. 4a–c). Due to its ingenious structure, the NiS_{NF}/CF@NiSNP−3 electrode yielded impressive results, with a remarkable specific capacitance of 1691.1 $F{\cdot}g^{-1}$ at 1 $A{\cdot}g^{-1}$, highlighting its exceptional ability to store electrical charge efficiently. Furthermore, it demonstrated a remarkable Coulombic efficiency of 98.5% (Fig. 4d, e). In addition, the cobalt sulfide electrode displayed excellent electrochemical performance in SCs. Peng et al. synthesized CoS_2 hollow nanospheres with adjustable internal structures using a one-step hydrothermal method [47]. Through the precise manipulation of the quantity of carbon disulfide, various types of CoS_2 (including solid, core–shell and double-shell) can be obtained. The results from the electrochemical tests unveiled the specific capacitance of the mesoporous CoS_2 hollow nanosphere (2–5 nm), which reached an impressive 1301 $F{\cdot}g^{-1}$ at 1 $A{\cdot}g^{-1}$. Remarkably, even after 2,000 cycles, the capacity retention remained as high as 90.1%.

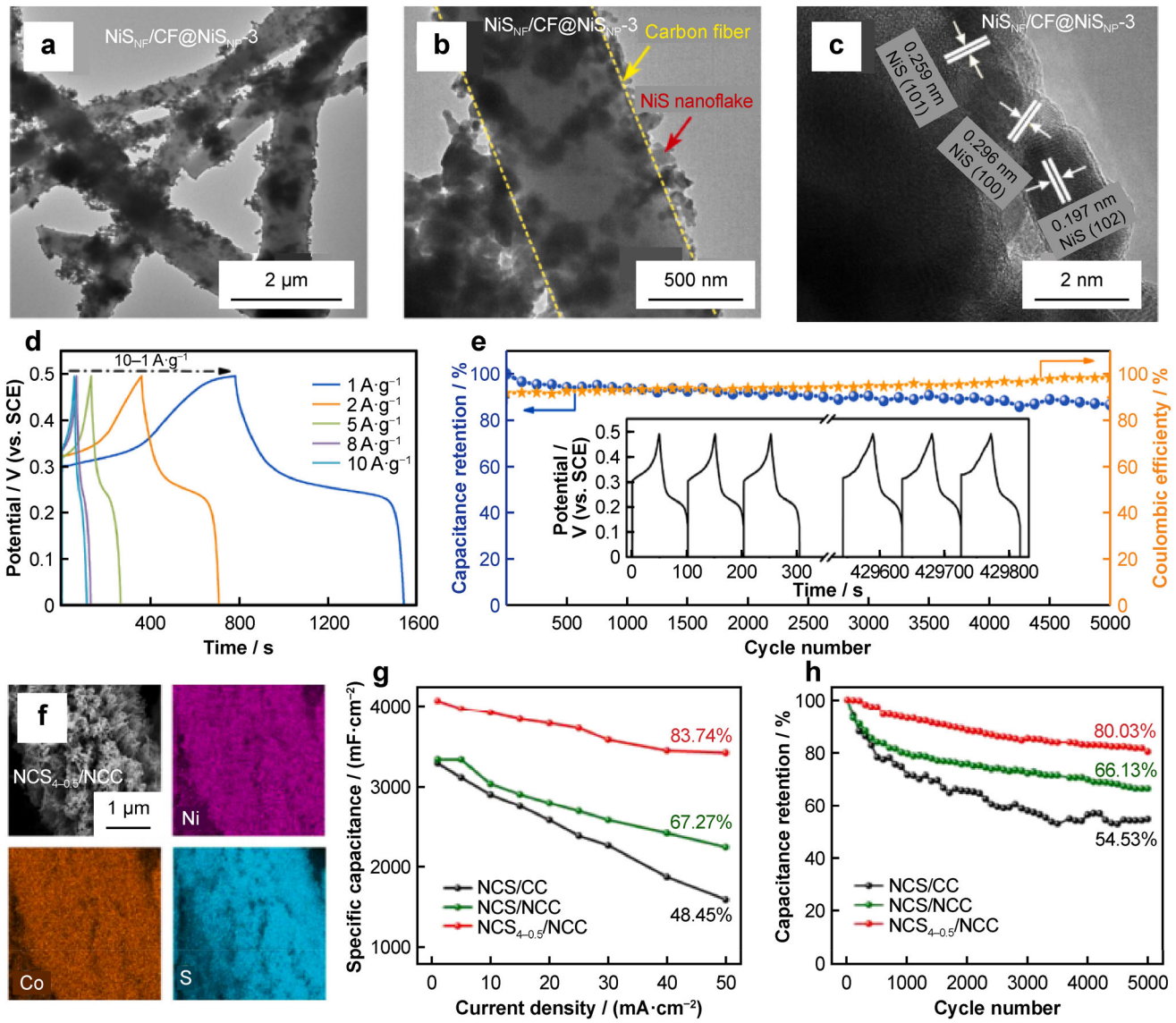

Fig. 4 Characterization and electrochemical evaluation of innovative electrode materials. **a–c** TEM images, **d** GCD curves and **e** cycle life curves of NiS_{NF}/CF@NiS_{NP}−3. Reproduced with permission from Ref. [70]. Copyright 2022, Elsevier. **f** SEM and EDS mapping images of $NCS_{4–0.5}$/NCC; **g** specific capacitance and **h** cycling stability of NCS/CC, NCS/NCC and $NCS_{4–0.5}$/NCC electrodes. Reproduced with permission from Ref. [71]. Copyright 2016, Wiley–VCH

Compared to individual metal sulfides, binary mixed-metal sulfides exhibit superior conductivity and provide a greater number of redox reaction sites. The synergistic effect between different elements has a significant influence on the electrochemical performance. Fully utilizing the advantages of the two metal elements can improve the electrochemical performance of electrode materials. For example, the presence of Ni increases the cell parameters *c* and a while reducing *c*/*a*, which helps improve the capacity. However, excessive Ni content can lead to the deterioration of cycling and rate performance, and the high pH value of high-nickel materials affects their actual use. Co can effectively stabilize the structure of electrode materials, suppress cation mixing, improve the electronic conductivity of materials, and improve the cycling performance. Therefore, utilizing the synergistic effect of Ni and Co will maximize the advantages of electrode materials for SCs, ensuring high-energy density, high magnification performance and long cycle life [71, 72]. Liu et al. [73] presented a dual-regulation strategy for developing high-performance electrode materials. This approach involved nitrogen doping of the CC (NCC) current collector and the introduction of sulfur vacancies in $NiCo_2S_4$ (NCS) (Fig. 4f). The $NCS_{4\text{-}0.5}$/NCC electrode benefited from the combined effect of NCC and sulfur vacancies, resulting in a remarkable specific capacitance of 4075.89 $mF{\cdot}cm^{-2}$ at 1 $mA{\cdot}cm^{-2}$ and exceptional cycling stability (Fig. 4g, h).

Transition metal sulfides are commonly found as nanoflowers, nanospheres, nanoflakes and nanorods. During frequent charge and discharge processes, NPs agglomerate easily, resulting in reduced capacity. In addition, fluctuation, expansion, thermodynamic instability, acid oxidation and volatility of metal sulfides are common problems in practical market applications. Therefore, efficient electrode structures must be developed.

2.3 Transition metal phosphide

Transition metal phosphides are n-type semiconductor materials with metal-like properties, rich redox reaction sites and excellent conductivities [74, 75]. Owing to the large radius of the phosphorus atoms, phosphides exhibit various crystal structures [76]. In addition, the low electronegativity of phosphorus ensures fast charge transfer [77]. Compared to transition metal compounds, transition metal phosphides are conducive to fast electron transport in SCs with a high-power density [78]. Transition metal phosphides include Co, Ni and Mo. Other transition metals, such as W, Mn and Cu, have been used to synthesize a variety of phosphides and have received increasing attention [37]. Typical single-transition metal phosphides include Co_2P, Ni_2P, Ni_5P_4 and Cu_3P. Zhou et al. [79] uniformly grew interconnected Ni_2P nanosheets on a Ni-foam surface, providing sufficient space for ion diffusion (Fig. 5a). The Ni_2P electrode achieved a specific capacitance of 3496 $F{\cdot}g^{-1}$ at 2.5 $A{\cdot}g^{-1}$ and retained a capacitance of 1109 $F{\cdot}g^{-1}$ at 83.3 $A{\cdot}g^{-1}$ (Fig. 5b). When cycled at a high current density of 10 $A{\cdot}g^{-1}$, the Ni_2P electrode exhibited rapid capacitance fading before 2,000 cycles, which may be caused by the reaction of the electrolyte and Ni_2P nanosheets to generate $Ni(OH)_2$. However, after 2,000 cycles, $Ni(OH)_2$ preserved the entire structure of Ni_2P and guaranteed good cycling stability (Fig. 5c).

Although most single-transition metal phosphides have good electrochemical capacity properties, their poor structural stability leads to lower rate performance and poor cycle stability, which is challenging for practical applications. Similar to transition metal oxides and sulfides, bimetallic phosphide materials play an important role. Binary metal phosphides usually have faster electronic conductivity, higher electrochemical reactivity and more abundant redox reaction sites than single transition metal phosphides, which are attributed to the synergy of the two transition metal elements. The two metal cations in the binary metal phosphide participate in the redox reaction, which has the advantage of producing a variety of oxidation states that will help store the charge and provide a higher capacity than a single-metal phosphide. Moreover, one metal cation in some binary metal phosphides participates in the redox reaction to contribute to the capacity, whereas another metal cation unrelated to the redox reaction facilitates electrochemical activity and enhances structural stability during the cycle, which considerably fosters the electrochemical performance of the entire material. Ding et al. [80] synthesized micro/nanostructured ternary Ni–Co–P materials for SCs using a one-pot solvothermal approach (Fig. 5d–g). Analysis via X-ray diffraction (XRD) revealed that the Ni_8–Co_1–P materials displayed distinct phases, including $M_{12}P_5$ and M_2P (M = Ni, Co) (Fig. 5h). Ni_8–Co_1–P outperformed the Ni–Co–P electrode in terms of the specific capacitance, rate capability and charge transfer kinetics. This superior performance can be attributed to the abundance of electroactive sites from Ni and Co on the electrode surface as well as the synergistic interaction between the Ni and Co redox species (Fig. 5i, j). Although transition metal phosphides have the above advantages, the phosphorus skeleton in a transition metal phosphide has high flexibility and various bonding modes, and there are often many phase components in its preparation process, making it challenging to synthesize pure phase transition metal phosphides.

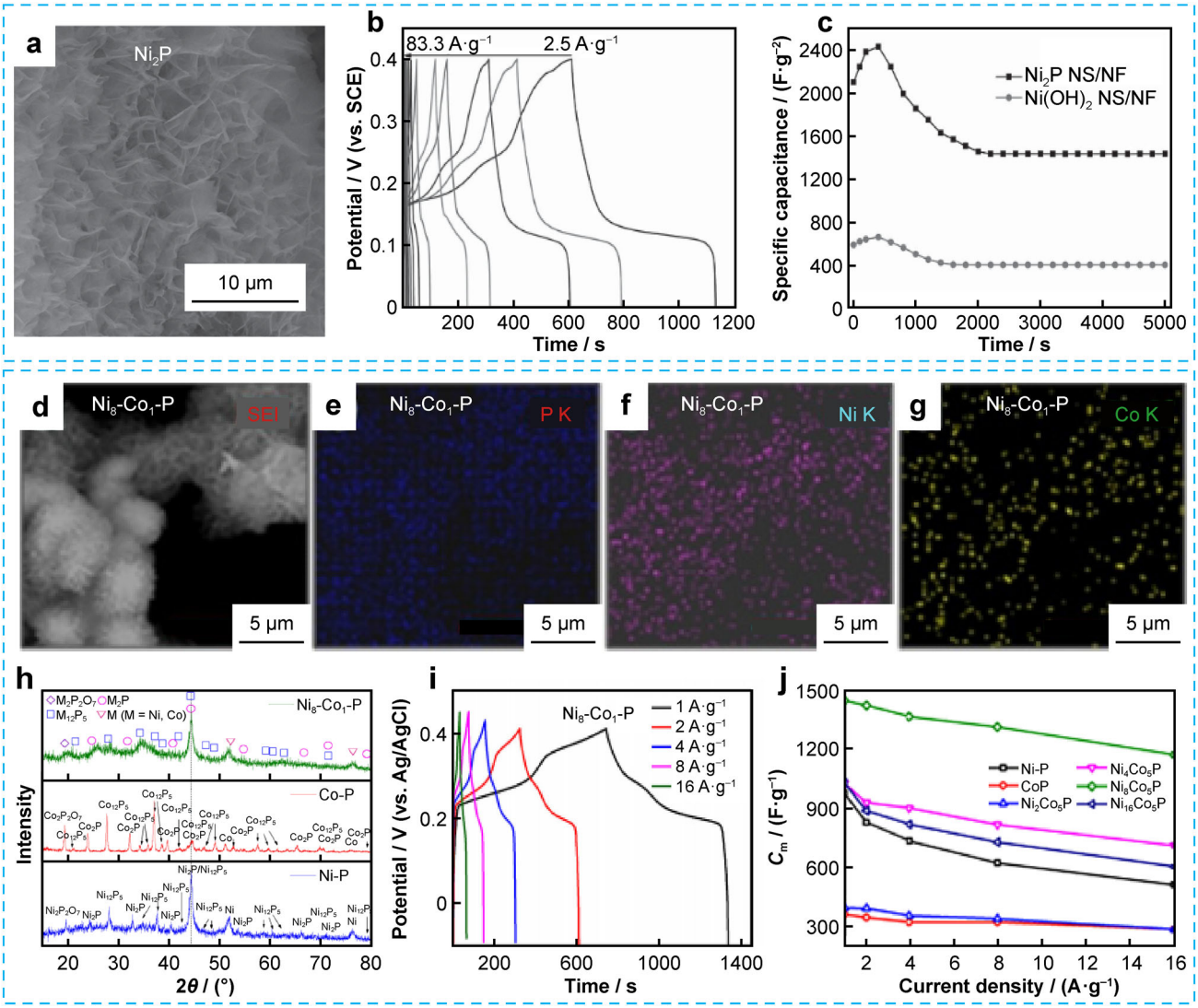

Fig. 5 **a** SEM image, **b** GCD curves and **c** cycling stability of Ni_2P. Reproduced with permission from Ref. [79]. Copyright 2015, Wiley–VCH. **d–g** TEM and EDS mapping images for Ni_8–Co_1–P materials; **h** XRD patterns for Ni_8–Co_1–P, Ni–P and Co–P electrode; **i** GCD curves of Ni_8–Co_1–P electrode; **j** rate performance of Ni–P, Co–P and Ni–Co–P (Ni/Co ratio = 16:1, 8:1, 4:1, 2:1) electrodes. Reproduced with permission from Ref. [80]. Copyright 2017, Elsevier

2.4 Transition metal selenide

Selenium, oxygen and sulfur are elements found in group VI-A of the periodic table. They shared the same number of valence electrons. Therefore, transition metal selenides have similar chemical properties to transition metal oxides and sulfides, suggesting that they have broad application prospects in SCs [81]. Moreover, selenium has better conductivity (1×10^{-3} S·m^{-1}) than O (1×10^{-5} S·m^{-1}) and S (1×10^{-28} S·m^{-1}) due to that e it has a larger radius and a smaller ionization energy, which ensure fast charge transfer. Transition metal selenides usually exhibit a 2D layered sandwich structure similar to that of graphite, with metal atoms located between the two selenide layers. This layered structure allows the simple reversible intercalation of other atoms in the interchain space so that energy can be easily stored without structural deformation, indicating its high rate performance and enhanced cycling stability. Recently, various single, binary, multinary and composite/hybrid/integrated metal selenides have been explored for SCs [82–90]. Among the various types of selenides, Ni_3Se_2 exhibits excellent electrical conductivity, a stable phase and robust physicochemical properties. These characteristics are closely linked to the composition, phase structure and morphology, as dictated by the phase diagram. Notably, in Ni_3Se_2, three Ni atoms are involved in a three-

electron reaction, leading to an increased capacity for charge storage. Therefore, Ni_3Se_2 is a promising candidate for an advanced electrode material [91]. Zhao et al. [92] synthesized a nanodendrite array of Ni_3Se_2 on nickel foam without a binder using a one-step hydrothermal method as a cathode material for SCs (Fig. 6a, b). The nanodendrite array Ni_3Se_2 on nickel foam exhibits a specific capacitance of 1234 $F{\cdot}g^{-1}$ at 1 $A{\cdot}g^{-1}$ (Fig. 6c, d). In comparison to single-metal selenides, binary- and multinary-metal selenides have more Faraday reaction sites and abundant structural defects owing to the coexistence and synergistic action of multiple metal ions and show better electrochemical performance. Qu et al. [93] synthesized a nanopolyhedral Ni–Co–Se electrode material with a hollow structure (Fig. 6e), which exhibited 1668 $F{\cdot}g^{-1}$ specific capacitance at 1 $A{\cdot}g^{-1}$ and high rate performance (Fig. 6f). Furthermore, Hosseini et al. [88] constructed a self-supporting porous Zn–Ni–Co/Cu selenide microsphere array on CC. The Zn–Ni–Co/Cu microball selenide exhibited a remarkable specific capacitance of 884.6 $C{\cdot}g^{-1}$ at 1 $A{\cdot}g^{-1}$ and an exceptional rate performance (Fig. 6g, h). However, the shortcoming of the volume effect (volume expansion or collapse) of transition metal selenides during the charging and discharging processes still needs to be overcome to improve their electrochemical performance and structural stability.

The data based on transition metal compounds as electrode materials for SC are shown in Table 1 [50, 53, 55, 58, 63, 66, 70, 79, and 80].

3 Synthetic methods and regulation strategies

3.1 Synthetic methods

The microstructure and properties of SC electrode materials are significantly affected by the thoughtful design, comprehensive research and precise control of the preparation process. Transition metal compounds can be synthesized using a range of preparation techniques, including hydrothermal/solvothermal, precipitation, electrodeposition, chemical vapor deposition (CVD) and sol–gel methods.

3.1.1 Hydrothermal/solvothermal method

The hydrothermal method involves synthesizing the precursor by dissolving and recrystallizing it in a closed-pressure reactor using water as the solvent under high-temperature and high-pressure conditions. The solvothermal method is a new material preparation method developed from the hydrothermal method that uses organic, amine or mixed solvents. The hydrothermal/solvothermal method involves transferring a prepared uniformly mixed solution to an autoclave, which is then placed in an oven to set the heating temperature and time. The microstructure of the material changed with changes in the hydrothermal time and temperature during the experiment. Zhang et al. [94] successfully used a hydrothermal method to synthesize 3D SnO_2 nanosheets on a CC substrate. As the

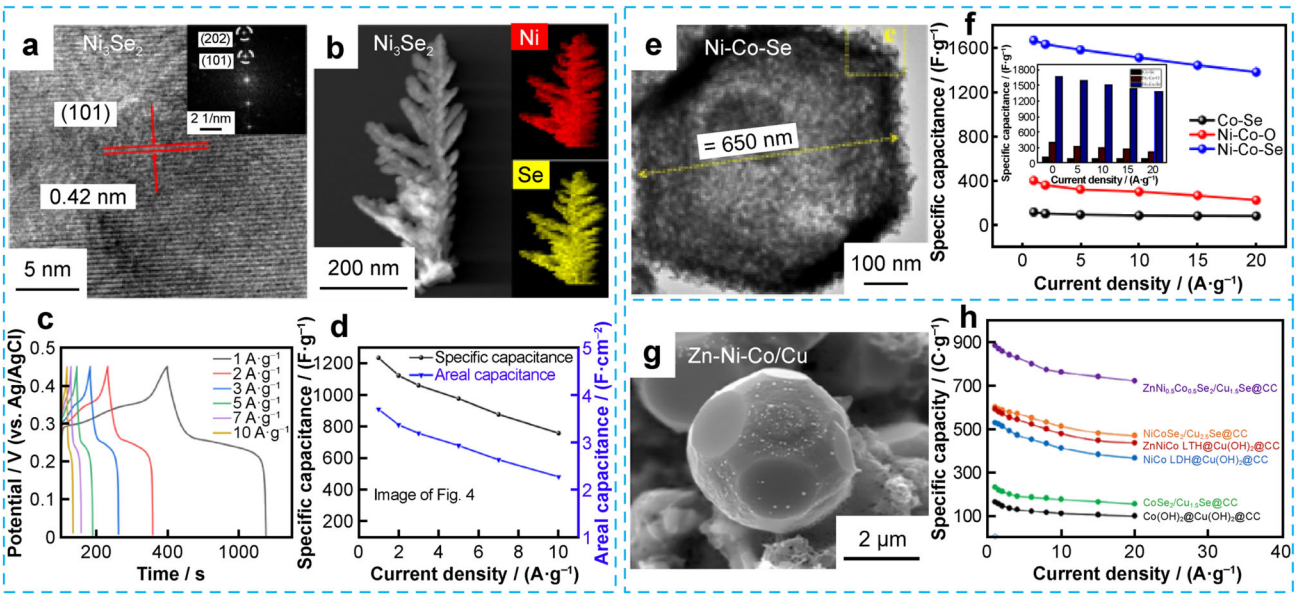

Fig. 6 Electrode characterization and specific capacitance analysis. **a** HRTEM and **b** mapping images, **c** GCD curves and **d** corresponding specific capacitance of Ni_3Se_2 electrode. Reproduced with permission from Ref. [92]. Copyright 2020, Elsevier. **e** TEM image and **f** specific capacitances of Ni–Co–Se electrode. Reproduced with permission from Ref. [93]. Copyright 2020, Elsevier. **g** SEM image and **h** specific capacitances of Zn–Ni–Co/Cu microballs selenide. Reproduced with permission from Ref. [88]. Copyright 2019, Elsevier

Table 1 Comparative data of transition metal compounds as electrode materials

Electrode material	Specific capacitance	Rate capability	Cycling performance	Refs.
RuO_2 nanorods	188 $F{\cdot}g^{-1}$ at 1 $mA{\cdot}cm^{-1}$	76.6%	3,000	[50]
	144 $F{\cdot}g^{-1}$ at 20 $mA{\cdot}cm^{-1}$		93.0%	
MnO_2 nanowires@CC	1174.3 $F{\cdot}g^{-1}$ at 2 $A{\cdot}g^{-1}$	78.9%	10,000	[53]
	927 $F{\cdot}g^{-1}$ at 40 $A{\cdot}g^{-1}$		99.9%	
1D/2D CoO	1178 $F{\cdot}g^{-1}$ at 0.5$A{\cdot}g^{-1}$	54.3%	3,000	[55]
	640 $F{\cdot}g^{-1}$ at 40$A{\cdot}g^{-1}$		93.1%	
α-$Ni(OH)_2$ nanosheets	562 $F{\cdot}g^{-1}$ at 10 $mV{\cdot}s^{-1}$	38.2%	500	[58]
	215 $F{\cdot}g^{-1}$ at 50 $mV{\cdot}s^{-1}$		62.0%	
$NiMoO_4$ Nanowires	3070 $F{\cdot}g^{-1}$ at 5 $mA{\cdot}cm^{-2}$	67.9%	50,000	[66]
	2085 $F{\cdot}g^{-1}$ at 100 $mA{\cdot}cm^{-2}$		96.0%	
hollow NiCo–LDHs	1877 $F{\cdot}g^{-1}$ at 1 $A{\cdot}g^{-1}$	61.3%	50,000	[63]
	1184 $F{\cdot}g^{-1}$ at 1 $A{\cdot}g^{-1}$		100%	
NiS_{NF}/CF@NiS_{NP}−3	1691.1 $F{\cdot}g^{-1}$ at 1 $A{\cdot}g^{-1}$	60.3%	5,000	[70]
	1020.3 $F{\cdot}g^{-1}$ at 10 $A{\cdot}g^{-1}$		86.8%	
Ni_2P NS/NF	3500 $F{\cdot}g^{-1}$ at 2.5 $A{\cdot}g^{-1}$	31.7%	5,000	[79]
	1109 $F{\cdot}g^{-1}$ at 83.3 $A{\cdot}g^{-1}$		68.4%	
Ni–Co–P	1448 $F{\cdot}g^{-1}$ at 1 $A{\cdot}g^{-1}$	81.0%	5,000	[80]
	1173 $F{\cdot}g^{-1}$ at 16 $A{\cdot}g^{-1}$		100%	

hydrothermal process progressed, the micromorphology of the material gradually transitioned from NPs to a nanosheet structure. Hydrothermal synthesis is used to produce nanomaterials of superior purity characterized by well-developed crystal structures. This approach effectively eliminates impurities and prevents structural defects that commonly arise during post-processing techniques such as high-temperature calcination or ball milling. However, this approach has limitations, such as the inability to directly observe the growth of crystals and synthesis of materials. In addition, this approach requires high-temperature and high-pressure equipment, corrosion-resistant linings, meticulous temperature control, substantial costs and safety concerns.

3.1.2 Precipitation method

The precipitation method precipitates insoluble compounds from water-soluble substances through a precipitation reaction, followed by subsequent treatment of the sediment, including direct precipitation, coprecipitation and uniform precipitation. The coprecipitation method involves homogeneously dissolving several kinds of cations in a solution and adding an appropriate amount of precipitator to induce the reaction and produce precipitation products with uniform composition. This is an effective method for synthesizing ultrafine powders containing several metal elements of composite oxides and hydroxides. This method has the advantages of mild reaction conditions, high product purity, easy industrial production, and easy nucleation control during the reaction process, and low cost. Xu et al. [95] synthesized $Ni_{0.75}Co_{0.15}Al_{0.1}(OH)_2$ using the coprecipitation method. The resulting $Ni_{0.75}Co_{0.15}Al_{0.1}(OH)_2$ electrode exhibited exceptional performance, even under an ultrahigh mass loading of 20.24 $mg{\cdot}cm^{-2}$. Furthermore, it displayed an excellent specific capacitance of 23.85 $F{\cdot}cm^{-2}$ at 10 $mA{\cdot}cm^{-2}$, along with a high rate capability (19.27 $F{\cdot}cm^{-2}$ at 40 $mA{\cdot}cm^{-2}$), indicating remarkable suitability for demanding applications. The electrode also exhibited outstanding cycling stability, highlighting its potential for long-term use. The precipitation method offers several benefits, including a straightforward preparation process, cost-effectiveness, ease of control over the synthetic conditions and a relatively short synthesis cycle. However, the addition of precipitation agents can potentially lead to excessively high local concentrations, which, in turn, may cause issues such as material agglomeration and uneven compositions during material synthesis.

3.1.3 Electrodeposition method

Electrodeposition involves a redox process in which positive and negative ions in an electrolyte solution migrate under the influence of an external electric field, leading to the formation of a coating on the electrode. The preparation of transition metal compounds by this method mainly involves introducing the desired metal

cations and anions, preparing a certain proportion of electrolytes in the electrolytic cell, and connecting the electrodes on a chemical workstation to carry out the electrodeposition process according to the different deposition processes. Simultaneously, nanomaterials with different properties can be prepared by changing the experimental conditions. Xu et al. [96] implemented an electrodeposition technique to grow Ni–Co–S nanosheets on an electrode composed of C–$NiCo_2O_4$/C nanowires. The resulting electrode demonstrated exceptional performance, including a high specific capacitance of 2396 $F{\cdot}g^{-1}$ at 3 $A{\cdot}g^{-1}$, impressive rate performance, and remarkable cycling stability of 92%. Electrodeposition can be used to obtain nanomaterials with various grain sizes, controllable material thicknesses, low cost and high efficiency. However, it is difficult to coat large workpiece areas.

3.1.4 CVD method

CVD technique involves the formation of solid deposits through the reaction of gaseous or vapor substances, either in the gas phase or at the gas–solid interface. This method mainly involves mixing two types of reactants (precursor and sulfur source, phosphorus source or selenium source) in a certain proportion in a tube furnace filled with inert gas or placing the sulfur source (phosphorus source or selenium source) upstream of the gas flow in the tube furnace and placing the precursor downstream to prepare transition metal sulfides (phosphide or selenide) at a constant temperature. Cheng et al. [97] phosphorylated $CoNi_2S_4$ into $CoNi_2S_4/Ni_3P$ electrode material by CVD method using NaH_2PO_2 as phosphorus source, which showed a high area-specific capacitance of 8.86 $F{\cdot}cm^{-2}$ at 3 $A{\cdot}g^{-1}$. CVD method does not have a deposition line of sight shadow and can deposit coatings on complex 3D workpieces at high deposition speeds. Thick coatings (sometimes up to a centimeter thick) can be obtained and the deposited coatings have good adhesion to the substrate. In addition, it has a good vacuum sealing performance and can be coated with high-melting-point materials at relatively low temperatures. It also has the advantage of controlling grain size and microstructure. However, this method also has a series of drawbacks, such as the need for volatile compounds in the reaction, which are unsuitable for commonly electroplated metals owing to the lack of suitable reactants such as tin, zinc and gold. Due to the release of highly toxic substances, corrosive exhaust gases and deposition reactions must be properly controlled and a closed system is required. The reactant utilization rate is low and the reaction is often limited by the equilibrium constant of the deposition reaction.

3.1.5 Sol–gel method

The sol–gel method employs precursors containing potent chemical compounds to initiate the process. This method uniformly mixes the active ingredients in a liquid phase and allows for chemical reactions, including hydrolysis and condensation. Consequently, a stable and transparent sol system is formed in the solution. This method offers several benefits, including simplicity of operation, affordability, the production of high-purity products, excellent uniformity and the ability to create abundant pore structures. Wei et al. [98] obtained a Co_3O_4 aerogel using a sol–gel method with subsequent drying and heat treatment. The isothermal adsorption–desorption test results showed that the Co_3O_4 aerogels obtained at different heat treatment temperatures contained mesopores. When the heat treatment temperature increases from 200 to 400 °C, the specific surface area of Co_3O_4 decreases from 235 to 69 $m^2{\cdot}g^{-1}$ and its specific capacitance decreases with the decrease of the specific surface area. Compared with alternative approaches, the sol–gel method exhibits an array of distinctive benefits. In this method, raw materials are dispersed and dissolved in a solvent, resulting in a low-viscosity solution. This characteristic enables the rapid achievement of molecular-level uniformity, ensuring efficient and thorough mixing of the reactants when the gel forms. Moreover, the requirement for solution reaction steps in the sol–gel method presents an opportunity to introduce trace elements easily and precisely. This method enables accurate and uniform doping at the molecular level, thereby facilitating an enhanced control of the process. In contrast to solid-state reactions, chemical reactions are more manageable and can be conducted at lower synthesis temperatures using the sol–gel method. However, it is essential to acknowledge that this technique has several challenges. First, the current selection of raw materials for the sol–gel process can be financially burdensome, with some containing organic substances that pose health risks. Moreover, the sol–gel procedure typically requires considerable time, often over several days or even weeks. Additionally, the presence of numerous micropores in the gel can trigger the release of substantial quantities of gases and organic substances during the drying phase, leading to subsequent contraction.

3.1.6 Other methods

In addition to the aforementioned conventional techniques, alternative approaches such as the microwave-assisted method, chemical bath deposition method and ion exchange method have been utilized to fabricate transition metal compounds. For example, Younas et al. [99] successfully synthesized Co–Se nanosheets using a

Table 2 Advantages and disadvantages of synthesis methods

Synthetic method	Advantages	Disadvantages
Hydrothermal/solvothermal method	Process is simple; Uniform product composition	Unable to observe crystal growth and material synthesis process; Safety issues (high-temperature and high-pressure)
Precipitation method	Mild conditions; beneficial to industrialization and production; low cost; high utilization rate of reactants; easy to control nucleation	Product is prone to agglomeration; uneven product composition
Electrodeposition method	Product composition is controllable; low cost; high efficiency	Difficulty in achieving large-scale layers
CVD method	High adhesion between coating and substrate; high product purity; controllable particle size	High requirements for reactants; low utilization rate of reactants; high cost
Sol–gel method	Simple process; low cost; easy to synthesize rich pores; mild conditions	Long synthesis time; pores are prone to shrinkage during drying process

microwave-assisted method. The results showed that the Co–Se electrode had a high specific capacitance of 1580 $F{\cdot}g^{-1}$ at 1 $A{\cdot}g^{-1}$. Patil et al. [100] prepared La_2Se_3 nanoflakes using chemical bath deposition. The maximum specific capacitance of the La_2Se_3 nanoflake electrode was 331 $F{\cdot}g^{-1}$ at 5 $mV{\cdot}s^{-1}$ and the specific capacitance remained 84% after 1,000 cycles. Chen et al. [101] prepared the precursor $NiCo_2(CO_3)_{1.5}(OH)_3$ on foam nickel by a hydrothermal method and then carried out a secondary hydrothermal ion exchange reaction with Na_2S to obtain $NiCo_2S_4$ nanotubes with a hollow structure. $NiCo_2S_4$ nanotubes electrode shows a very high area-specific capacitance (14.39 $F{\cdot}cm^{-2}$).

The advantages and disadvantages of the synthesis method are shown in Table 2.

3.2 Regulation strategies

Based on the above problems with transition compounds, three strategies have been proposed to improve their electrochemical performance: (1) regulation of nanostructures, (2) interface engineering and (3) design of composite electrodes.

3.2.1 Regulation of nanostructures

The morphology and nanostructure of electrode materials significantly affect the practicability area, diffusion path of the electrolyte ions and structural stability. There are many ways to construct nanomaterials with special structures and morphologies: 1D nanorods or nanowires, which increase the conductivity of ions or electrons, 2D nanosheets which increase the active area; and design 3D hierarchical nanomaterials [102, 103]. They also include nanospheres, octahedral and cubes. All types of special structures (such as porous structures, micron/nano hierarchical structures, hollow structures and core–shell structures) can significantly increase the specific surface area of the material, facilitate the penetration of electrolytes, shorten the propagation path of ions and electrons, and alleviate the volume change caused during the charge–discharge process [104–107].

Owing to the good conductivity of 1D nanowires, Rauf et al. [108] prepared ZnS nanowires with a large aspect ratio using a one-step hydrothermal method (Fig. 7a–c). The ZnS nanowires interconnected to form a 3D network structure that facilitated electrolyte diffusion toward the material surface and improved the utilization of the active materials. In addition, the fine nanowire characteristics of ZnS promotes the diffusion of electrolytes in the internal region of the electrode, thereby reducing the internal resistance. The contact area between the electrodes and electrolyte can also increase the number of ion adsorption sites for charge transfer. The obtained ZnS nanowire electrode showed a specific capacitance of 781 $F{\cdot}g^{-1}$ at 0.5 $A{\cdot}g^{-1}$. 2D nanosheets with nanoscale thicknesses and microscale lateral dimensions displayed extraordinary morphological anisotropy, leading to an increased surface area. 2D nanomaterials have no interlayer contacts owing to electronic confinement and display better electronic properties than other nanomaterials [109]. Liu et al. [110] reported a nanosheet array of nickel–cobalt selenide ($(Ni,Co)Se_2$) with a hierarchical NP/nanosheet structure, which was grown on an acidified CC substrate via hydrothermal and selenization processes (Fig. 7d–f). The nanosheet array $(Ni,Co)Se_2$ had a rough and porous surface, which increased the contact area between the electrode and electrolyte and supplied more active sites. The

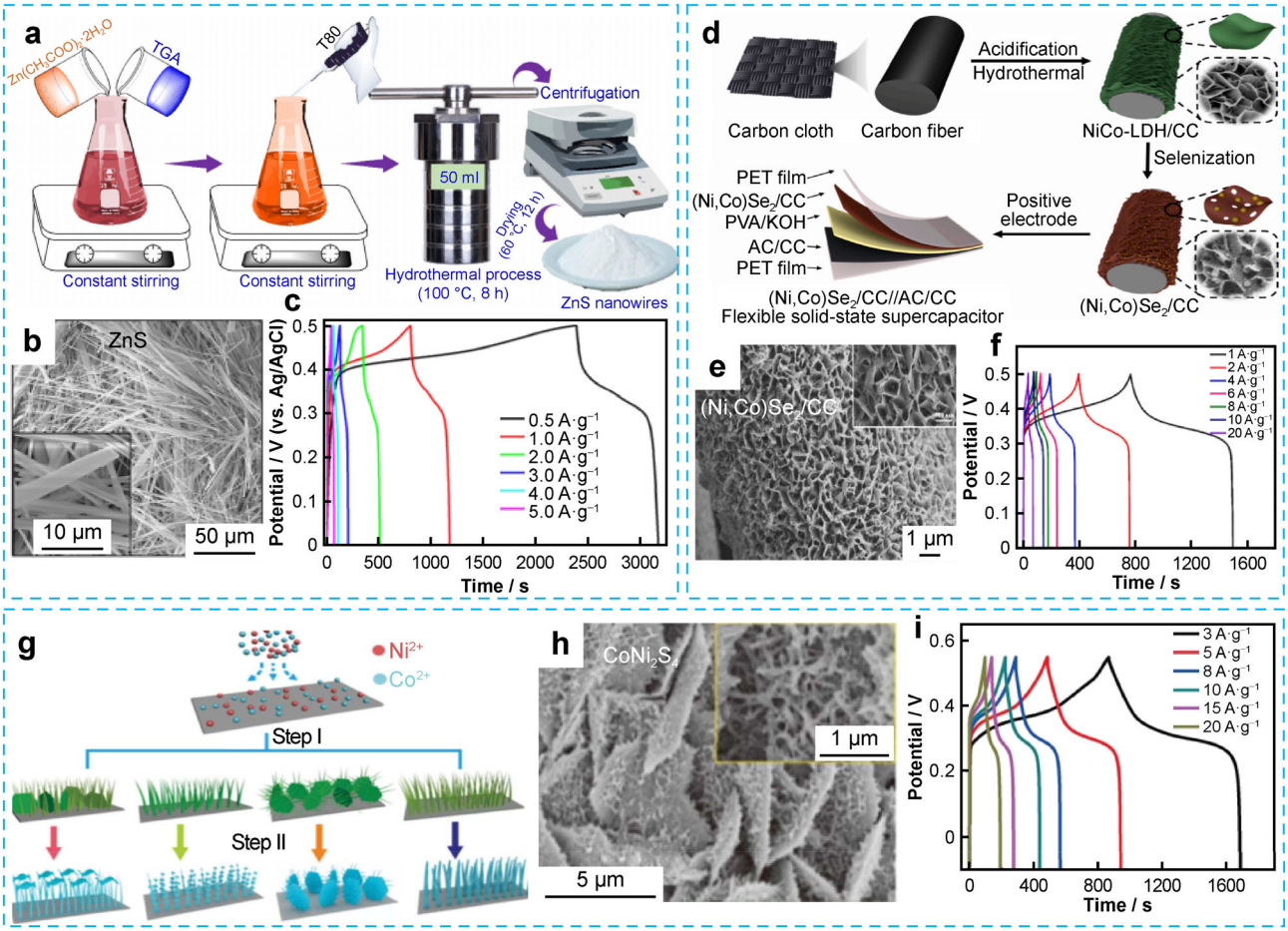

Fig. 7 Synthesis and characterization of nanowires and nanoarrays. **a** Schematic diagram for hydrothermal synthesis, **b** SEM image, and **c** GCD curves of ZnS nanowires. Reproduced with permission from Ref. [108]. Copyright 2022, Elsevier. **d** Schematic diagram for synthesis process of (Ni,Co)Se_2/CC nanoarrays; **e** SEM image and **f** GCD curves of (Ni,Co)Se_2/CC. Reproduced with permission from Ref. [110]. Copyright 2023, Elsevier. **g** Schematic illustration of Co–Ni–S by hydrothermal process; **h** SEM images and **i** GCD curves of $CoNi_2S_4$. Reproduced with permission from Ref. [111]. Copyright 2020, The Royal Society of Chemistry

(Ni,Co)Se_2/CC electrode showed a high specific capacitance of 2054 $F{\cdot}g^{-1}$ at 1 $A{\cdot}g^{-1}$ and excellent rate performance of 90.3% retention at 10 $A{\cdot}g^{-1}$. A 3D structure can incorporate many nano-components into microscale structures, such as 3D micro-nanostructures interwoven by nanosheet structures and nanowire structures, while sustaining the unique performance of the components at the nanoscale. Han et al. [111] reported a $CoNi_2S_4$ electrode consisting of 2D microsheets and 1D nanowires, which were ornamented by 2D ultrathin nanosheets homogeneously covering the surface of the Ni foam, forming an architecture with a 3D porous structure using a two-step hydrothermal method (Fig. 7g–i). The $CoNi_2S_4$ electrode displayed an enhanced specific capacitance (3784.6 $F{\cdot}g^{-1}$ at 3 $A{\cdot}g^{-1}$) and extraordinary rate capability (2932.3 $F{\cdot}g^{-1}$ at 20 $A{\cdot}g^{-1}$). The exceptional electrochemical performance can be attributed to the benefits derived from the multidimensional structure formed through the interconnection of the 2D microsheets, 1D nanowires and 2D ultrathin nanosheets. This structural arrangement offers abundant active sites and provides a substantial contact area at the electrode/electrolyte interface, thereby significantly enhancing the transport kinetics of electrons and ions.

3.2.2 *Interface engineering*

The interface between the current collector and active materials is important for effective electron transmission; as the structure without a binder has better electrical contact, an array of active materials can be directly grown on the substrate. The active material with an array structure is grown in situ on the current collector, which can avoid the "dead surface" owing to that it introduces polymer binder and conductive agent, reduces the contact resistance, maximizes the use of the active materials, and improves the interface of the active materials/current collector to achieve fast and effective electronic transmission. Compared with traditional powder samples, the capacitance performance

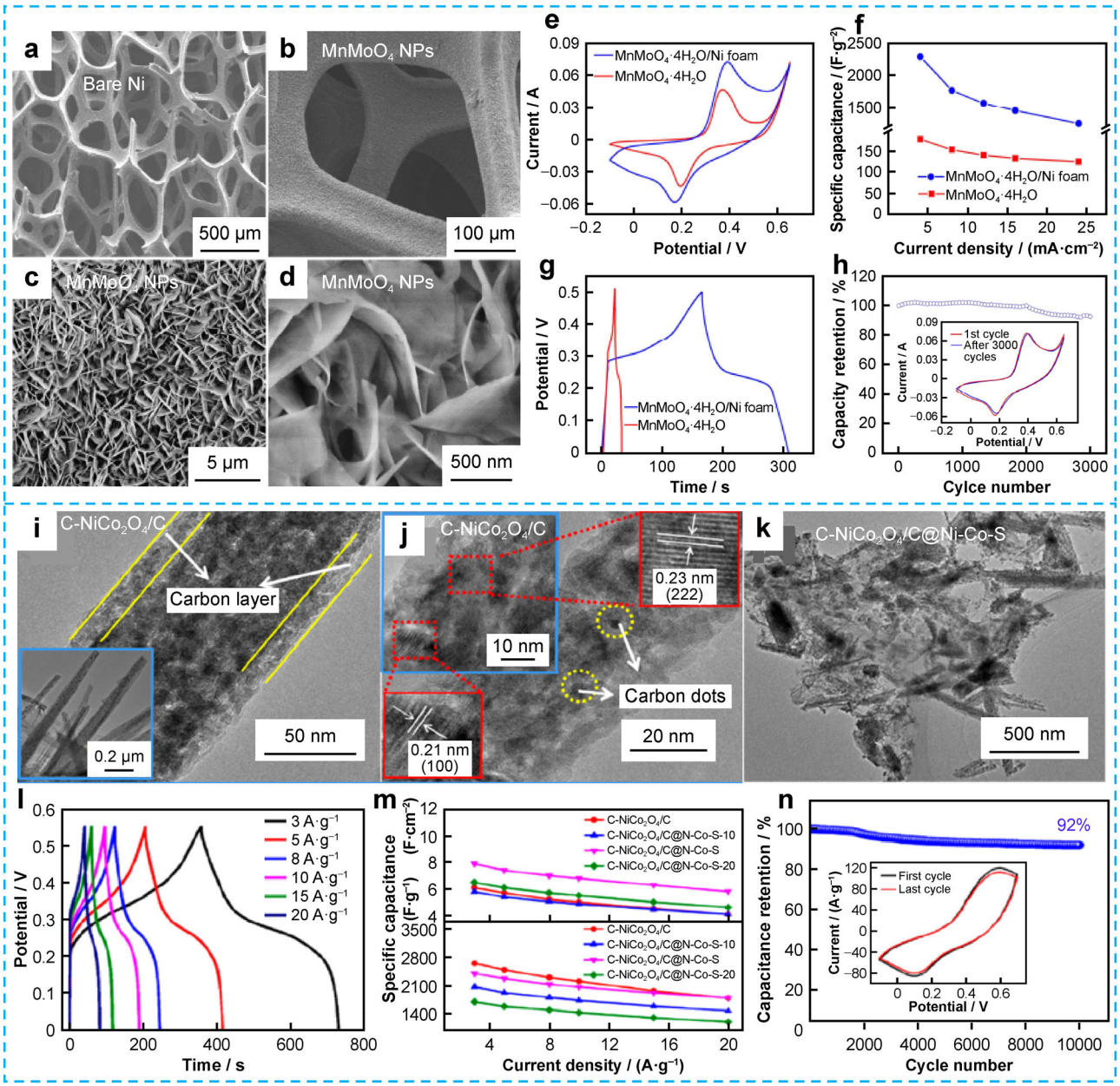

Fig. 8 Morphological characterization and electrochemical performance of $MnMoO_4$ NPs on Ni Foam and C–$NiCo_2O_4$/C@Ni–Co–S electrode. SEM images of **a** bare Ni foam and **b–d** $MnMoO_4$ NPs grown directly on Ni foam; **e** CV curves, **f** rate performance, **g** GCD curves and **h** cycling performance of $MnMoO_4$ NPs grown on Ni foam. Reproduced with permission from Ref. [112]. Copyright 2014, The Royal Society of Chemistry. **i** TEM and **j** HRTEM images of C–$NiCo_2O_4$/C nanowires; **k** TEM images, **l** GCD curves of C–$NiCo_2O_4$/C@Ni–Co–S electrode; **m** rate capacitance of C–$NiCo_2O_4$/C, C–$NiCo_2O_4$/C@Ni–Co–S–10, C–$NiCo_2O_4$/C@Ni–Co–S, and C–$NiCo_2O_4$/C@Ni–Co–S–20 electrode; **n** cycling retention of C–$NiCo_2O_4$/C@Ni–Co–S electrode. Reproduced with permission from Ref. [96]. Copyright 2021, ACS Publications

was greatly improved by designing NP, nanowire, nanotube and nanosheet structures. Cao et al. [112] prepared $MnMoO_4$ nanoplates grown directly on Ni foam using a hydrothermal method (Fig. 8a–d). Figure 8e shows CV curves of the pure $MnMoO_4$ powder and $MnMoO_4$ NPs on Ni foam at 50 $mV{\cdot}s^{-1}$, demonstrating that the $MnMoO_4$ NP electrode on Ni foam had a higher specific capacitance than the pure $MnMoO_4$ powder electrode (Fig. 8f). As integrated electrodes for SCs, the $MnMoO_4$ nanoplate electrode supported directly on Ni foam exhibited good electrochemical performances with a high specific capacitance of 1.15 $F{\cdot}cm^{-2}$ (2300 $F{\cdot}g^{-1}$ at 4 $mA{\cdot}cm^{-2}$ and a good cyclic stability (92% capacity retention rate after 3,000 cycles) (Fig. 8g, h). This remarkable electrochemical

performance can be ascribed to the porous structure formed by the interconnected $MnMoO_4$ nanoplates. This structure enhances the efficiency of electrolyte diffusion and promotes electron transport, thereby contributing to an overall superior electrochemical performance.

In addition, the introduction of a buffer layer between the active materials and substrate can facilitate rapid electron collection and transport, improving the electrochemical performance of the electrode materials. Xu et al. [96] designed a C–$NiCo_2O_4$/C@Ni–Co–S electrode by coupling zero-dimensional (0D)/2D carbon-modified $NiCo_2O_4$ in the interior with Ni–Co–S nanosheets in the external sheath (Fig. 8i–k). By incorporating 0D carbon doping, the agglomeration of $NiCo_2O_4$ NPs was effectively inhibited, leading to enhanced electronic conductivity. A C–$NiCo_2O_4$ nanowire array was used as the skeleton and scaffold to prevent the aggregation of the Ni–Co–S nanosheets, thus exposing more active sites. The ultrathin 2D carbon intermediate layer on the surface of the C–$NiCo_2O_4$ nanowire can supply fast electronic channels for charge storage and transportation, and the perfect Ni–Co–S nanosheets can coat on the surface of C–$NiCo_2O_4$ nanowire array as a "protection" layer, thus improving the stability of the nanowire structure. C–$NiCo_2O_4$/C@Ni–Co–S electrode delivers a high specific capacitance of 2396 $F{\cdot}g^{-1}$ at 3 $A{\cdot}g^{-1}$ and good cycling stability (Fig. 8l–n).

Another remarkable interface engineering technique is the direct growth of a core–shell array on the current collector, which has an interconnected network structure that provides efficient ion/electron transportation and alleviates volume variation. Moreover, the core–shell nanostructure can integrate two active materials and inherit the advantages of "core" material and "shell" material. Zhang et al. [113] successfully synthesized hierarchical core–shell $CoMoO_4$@$NiMoO_4$ nanosheet arrays on Ni foam using a two-step hydrothermal method and calcination (Fig. 9a–c). The $CoMoO_4$@$NiMoO_4$ composite electrode displayed an excellent specific capacitance of 1639.8 $F{\cdot}g^{-1}$, which was higher than those of the $CoMoO_4$ and $NiMoO_4$ electrodes (Fig. 9d, e) due to its larger specific surface area and increased number of active sites. Adhikari et al. [114] successfully prepared a binder-free 2D/2D $FeCo_2O_4$@-$Ni(OH)_2$ material with a core–shell structure grown on the Ni foam, in which $FeCo_2O_4$ microsheets are as "core" and $Ni(OH)_2$ nanosheets are as "shell" (Fig. 9f). SEM image shows that $FeCo_2O_4$ has a microsheet structure and the high-magnification image shows that the thickness of the microsheet is 289 nm (Fig. 9g, h). After coating with $Ni(OH)_2$, the thickness of $FeCo_2O_4$@$Ni(OH)_2$ increased to 310 nm (Fig. 9i, j). The $FeCo_2O_4$@$Ni(OH)_2$ electrode displayed an excellent specific capacitance of 1944 $F{\cdot}g^{-1}$ at 5 $A{\cdot}g^{-1}$, which was higher than the specific capacitance of $FeCo_2O_4$ and $Ni(OH)_2$ electrodes (Fig. 9k, l).

3.2.3 Design of composite electrode materials

It is difficult for a single material to simultaneously balance the high specific capacity, good cycling stability and high energy/power densities. Therefore, researchers have shifted their focus to composite electrode materials and have used the synergy of composite electrode materials to improve the comprehensive performance of electrode materials. Due to the low conductivity and cycle stability of transition metal compounds, carbon materials with high conductivity and perfect material stability are used for composites. The excellent performance of these composite materials is mainly due to that carbon can inhibit the aggregation of transition metal compounds, offer a large accessible surface area, and reduce the volume change of the composite material during the charging-discharging process to improve the stability of the electrode material. In addition, the good conductivity of carbon compensates for the influence of the low conductivity of transition metal compounds. Various transition metal compounds with different morphologies have been combined with carbon materials to form composite electrode materials. For example, Sun et al. [115] prepared α-$Ni(OH)_2$ nanosheet arrays modified by carbon quantum dots using a one-step hydrothermal method (CQDs/α-$Ni(OH)_2$). SEM images in Fig. 10a, b show that the morphology of $Ni(OH)_2$ is similar to that of CQDs/α-$Ni(OH)_2$. Notably, the surface of CQDs/α-$Ni(OH)_2$ is rougher, suggesting that the addition of CQDs can raise the specific surface area, leading to exposure of the active site. Transmission electron microscopy (TEM) images of CQDs/α-$Ni(OH)_2$ in Fig. 10c, d show the introduction of CQDs into α-$Ni(OH)_2$. The optimized electrode has a specific capacitance of 1724.0 $F{\cdot}g^{-1}$ at 3 $A{\cdot}g^{-1}$, which is 2.3 times that of bare α-$Ni(OH)_2$. (Fig. 10e, f) The hierarchical structure of α-$Ni(OH)_2$ and the aid of CQDs enhanced the reaction sites of CQDs/α-$Ni(OH)_2$ and increased conductivity, thus obtaining high electrochemical performances.

In addition, composite electrode materials consisting of two different transition metal compounds, in which one compound acts as a skeleton for the growth of the other compounds to generate the array structure, have been extensively studied. This composite structure effectively prevents the accumulation of electroactive materials. This is particularly instructive for practical applications in which a high-energy density can be achieved even when high loads normally require the use of SCs. Yuan et al. [116] successfully combined a highly electronically conductive $NiCo_2O_4$

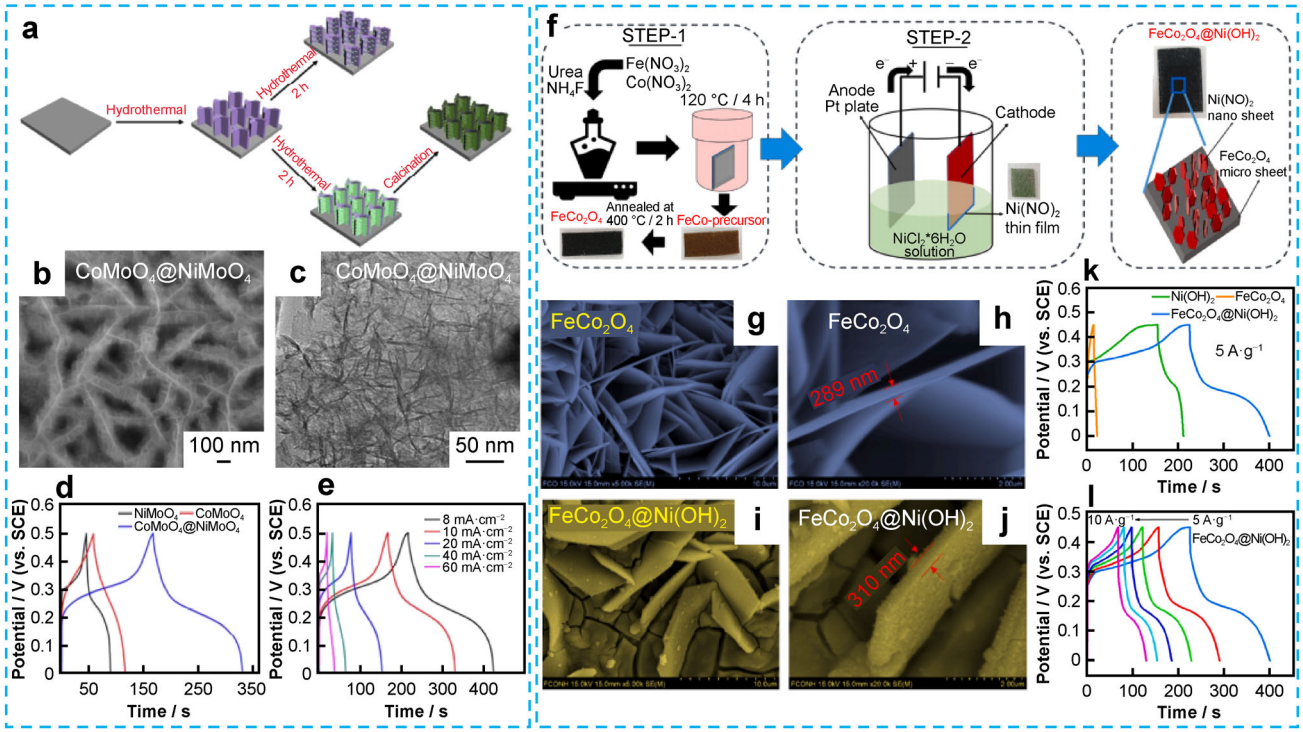

Fig. 9 **a** Diagrammatic sketch of hierarchical core–shell $CoMoO_4$@$NiMoO_4$ nanosheet array synthesis process; **b** SEM and **c** TEM images of $CoMoO_4$@$NiMoO_4$; GCD curves of **d** $CoMoO_4$, $NiMoO_4$, $CoMoO_4$@$NiMoO_4$ and **e** $CoMoO_4$@$NiMoO_4$ electrode. Reproduced with permission from Ref. [113]. Copyright 2021, The Royal Society of Chemistry. **f** Diagrammatic sketch of $FeCo_2O_4$@$Ni(OH)_2$ electrode preparation; SEM images of **g, h** $FeCo_2O_4$ and **i,j** $FeCo_2O_4$@$Ni(OH)_2$ core–shell arrays; GCD curves of **k** $FeCo_2O_4$, $Ni(OH)_2$, $FeCo_2O_4$@$Ni(OH)_2$ and **l** $FeCo_2O_4$@$Ni(OH)_2$ electrode. Reproduced with permission from Ref. [114]. Copyright 2023, Elsevier

material with a high-capacitance $MnMoO_4$ material. SEM images in Fig. 10g, h show the morphology and structure of the as-prepared $NiCo_2O_4$ and $NiCo_2O_4$@$MnMoO_4$ electrode materials, respectively. $NiCo_2O_4$ nanowires were densely coated on foam nickel in a multitudinous space. Each $NiCo_2O_4$ nanowire is about 100 nm in diameter and over 1 μm in length. TEM results revealed the detailed structure of the $NiCo_2O_4$ nanowires and $NiCo_2O_4$@$MnMoO_4$ nanocolumns (Fig. 10i–l). $NiCo_2O_4$ nanowires consist of numerous interconnected NPs with diameters of ~ 50 nm. TEM images of the $NiCo_2O_4$@$MnMoO_4$ nanocolumn showed that the $NiCo_2O_4$ nanowires were covered with a large number of $MnMoO_4$ nanosheets. The $NiCo_2O_4$@$MnMoO_4$ nanoarray electrode exhibited an excellent capacitance of 1169 $F{\cdot}g^{-1}$ at 2.5 $mA{\cdot}cm^{-2}$, obviously higher than those of the pristine $NiCo_2O_4$ and $MnMoO_4$ electrodes (Fig. 10m–o). The excellent electrochemical performance of the $NiCo_2O_4$@$MnMoO_4$ electrode is mainly due to the increase in its specific surface area, abundance of electroactive sites, fast electron and ion transport paths, and synergistic effect of the $NiCo_2O_4$ and $MnMnO_4$ electrode materials.

The advantages and disadvantages of the regulation strategies are shown in Table 3.

4 Conclusions and prospects

This study reviewed the research progress, existing problems and repair strategies of transition metal compounds as electrode materials for SCs. Currently, the main transition metal compounds used as electrode materials for SCs are oxides/hydroxides, sulfides, phosphides and selenides. Although progress has been made in using transition metal compounds as electrode materials for SCs, their development has been hindered by shortcomings. For example, pure-phase electrode materials are expensive to manufacture, complex to synthesize, and exhibit poor conductivity. Powder electrode materials easily agglomerate during electrochemical tests, resulting in a small specific surface area. The specific capacitance and cycle stability of nanomaterials are severely limited by their volume expansion/contraction during frequent charging and discharging processes. Thus, to prepare transition metal compound electrode materials with excellent electrochemical properties, researchers have proposed many strategies, including the improvement of synthetic methods, regulation of nanostructures, interface engineering and synthesis via the synergistic effect of nanomaterials.

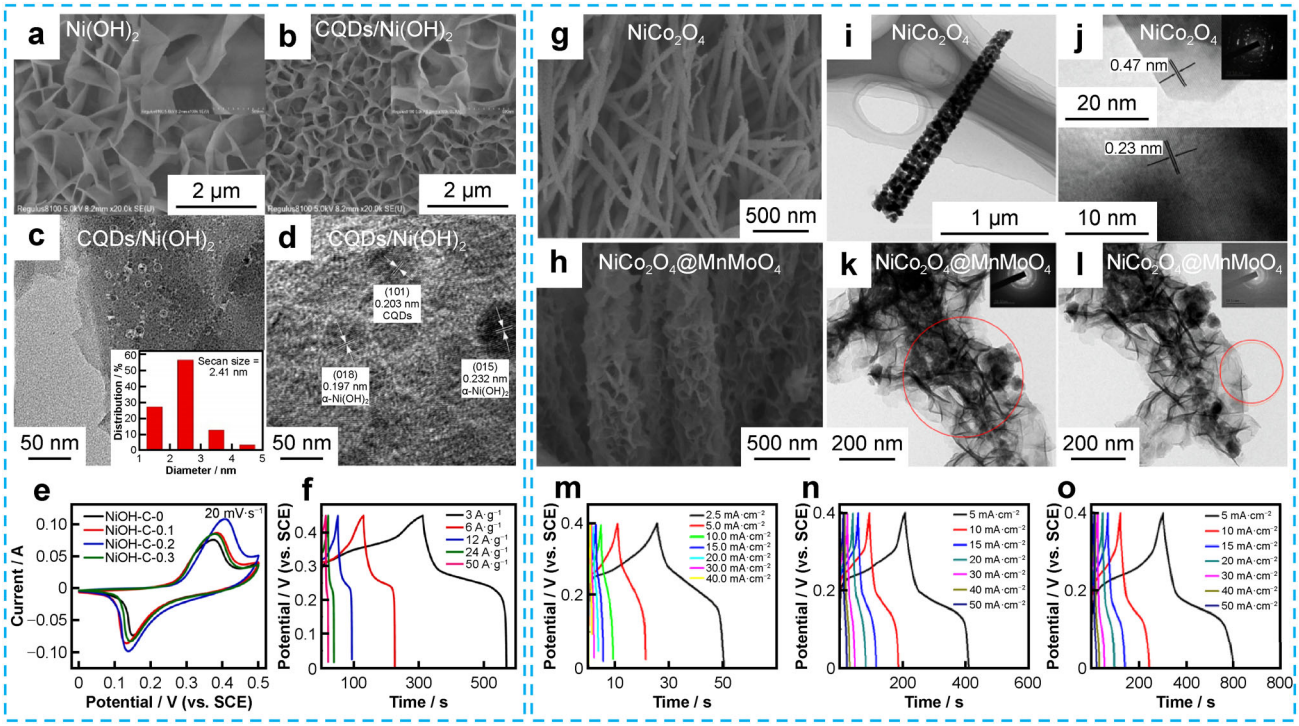

Fig. 10 SEM images of **a** $Ni(OH)_2$ and **b** CQDs/$Ni(OH)_2$; **c, d** TEM images of CQDs/$Ni(OH)_2$; **e** CV curves and **f** GCD curves of CQDs/$Ni(OH)_2$ electrode. Reproduced with permission from Ref. [115]. Copyright 2023, Elsevier. SEM images of **g** $NiCo_2O_4$ nanowires and **h** $NiCo_2O_4$@$MnMoO_4$ nanocolumns; TEM images of **i**, **j** $NiCo_2O_4$ nanowires and **k**, **l** $NiCo_2O_4$@$MnMoO_4$ nanocolumns; GCD curves of **m** $MnMoO_4$, **n** $NiCo_2O_4$ and **o** $NiCo_2O_4$@$MnMoO_4$. Reproduced with permission from Ref. [116]. Copyright 2017, ACS Publications

Table 3 Advantages and disadvantages of regulation strategies

Regulation strategy	Advantages	Disadvantages
Regulation of nanostructures	1D: increase ion/electron conductivity 2D: increase active area 3D: promote electrolyte penetration and alleviate volume expansion	Difficulty in achieving targeted synthesis of certain nanostructures
Interface engineering	Avoid dead volume and reduce contact resistance	Some materials cannot grow directly on substrate and require action of binders
Design of composite electrode materials	Synergistic effect of two or more materials can be utilized	Multiple synthesis steps and long cycle

Despite considerable progress in the use of transition metal compounds as electrode materials for SCs through various improvement strategies, there is still a large gap between laboratory research results and commercial applications and many challenges faced by SCs are yet to be solved. 1) Although many metals can form transition metal compounds, their practical applications are limited and mainly concentrated in Ni– and Co-based materials. Material properties can be predicted theoretically using computer science. Therefore, more efficient transition metal compounds will be synthesized and show great prospects in the future. 2) Elemental doping can adjust the electronic state of transition metal compounds and the adsorption properties of the reactants, thereby altering the activity and selectivity of the reaction and promoting the conductivity of transition metal compounds. However, the doping elements are limited to a few elements such as O and N. Apart from cation doping, anion doping also needs to be further explored. 3) A more in-depth exploration of the energy storage mechanism is needed to provide theoretical support for the more targeted and accurate design of electrode materials. 4) It is necessary to develop more advanced characterization techniques to determine the intrinsic causal relationships of the material composition, structure and properties from the macro to the micro level and the molecular to the atomic level. 5) The construction

of high-mass-loading electrodes and structures should be further studied as it is an important step in bridging the gap between laboratory and commercialization.

Acknowledgements This work was financially supported by the National Natural Science Foundation of China (No. 22301151), the Natural Science Foundation of Inner Mongolia Autonomous Region of China (No. 2022QN05024), the Fundamental Scientific Research Funds for Universities directly under Inner Mongolia Autonomous Region of China (Nos. JY20230097 and JY20220116), the Program for Innovative Research Team in Universities of Inner Mongolia Autonomous Region (No. NMGIRT2211), Inner Mongolia University of Technology Key Discipline Team Project of Materials Science (No. ZD202012) and the Young Leading Talent of "Grassland Talents" Project of Inner Mongolia Autonomous Region (No. QNLJ012010).

Declarations

Conflict of interests The authors declare that they have no conflict of interest.

References

[1] Zhang Y, Xu J, Zheng YY, Zhang YJ, Hu X, Xu TT. Construction of $CuCo_2O_4$@$CuCo_2O_4$ hierarchical nanowire arrays grown on Ni foam for high-performance supercapacitors. RSC Adv. 2017;7:3983. https://doi.org/10.1039/C6RA25970G.

[2] Zhang YN, Su CY, Chen JL, Huang WH, Lou R. Recent progress of transition metal-based biomass-derived carbon composites for supercapacitor. Rare Met. 2023;42(3):769. https://doi.org/10.1007/s12598-022-02142-7.

[3] He J, Wang HP, Zhou Q, Qi SH, Wu M, Li F, Hu W, Ma JM. Unveiling the role of Li^+ solvation structures with commercial carbonates in the formation of solid electrolyte interphase for lithium metal batteries. Small Methods. 2021;5:2100441. https://doi.org/10.1002/smtd.202100441.

[4] Gao L, Zhang LL, Yang XL. N, S-codoped porous carbon nanosheets decorated with Fe_3C nanoparticles as high-performance anode materials for lithium ion hybrid supercapacitors. Rare Met. 2022;41(7):2517. https://doi.org/10.1007/s12598-021-01927-6.

[5] Liang H, Su M, Zhao X, Gu Z, Yang J, Guo W, Liu Z, Zhang J, Wu X. Weakly-solvating electrolytes enable ultralow-temperature (− 80 °C) and high-power CF_x/Li primary batteries. Sci China Chem. 2023;66:1982. https://doi.org/10.1007/s11426-023-1638-0.

[6] Yang J, Zhao X, Zhang W, Ren K, Luo X, Cao J, Zheng S, Li W, Wu X. "Pore-hopping" ion transport in cellulose-based separator towards high-performance sodium-ion batteries. Angew Chem Int Ed. 2023;62: e202300258. https://doi.org/10.1002/ange.202300258.

[7] Aravindan V, Gnanaraj J, Lee YS, Madhavi S. Insertion-type electrodes for nonaqueous Li-ion capacitors. Chem Rev. 2014;114:11619. https://doi.org/10.1021/cr5000915.

[8] Dunn B, Kamath H, Tarascon JM. Electrical energy storage for the grid: a battery of choices. Science. 2011;334:928. https://doi.org/10.1126/science.1212741.

[9] Zhu Y, Murali S, Stoller MD, Ganesh KJ, Cai W, Ferreira PJ, Pirkle A, Wallace RM, Cychosz KA, Thommes M, Su D, Stach EA, Ruoff RS. Carbon-based supercapacitors produced by activation of graphene. Science. 2011;332:1537. https://doi.org/10.1126/science.1200770.

[10] Yao JJ, Liu C, Li JY, Hu ZL, Zhou RY, Guo CC, Liu XR, Yang FF, Zhu YR. 3D nitrogen and boron dual-doped carbon quantum dots/reduced graphene oxide aerogel for advanced aqueous and flexible quasi-solid-state zinc-ion hybrid capacitors. Rare Met. 2023;42(7):2307. https://doi.org/10.1007/s12598-023-02265-5.

[11] Qi JQ, Huang MY, Ruan CY, Zhu DD, Zhu L, Wei FX, Sui YW, Meng QK. Construction of CoNi2S4 nanocubes interlinked by few-layer $Ti_3C_2T_x$ MXene with high performance for asymmetric supercapacitors. Rare Met. 2022;41(12):4116. https://doi.org/10.1007/s12598-022-02167-y.

[12] Sharma P, Bhatti TS. A review on electrochemical double-layer capacitors. Energ Convers Manage. 2010;51:2901. https://doi.org/10.1016/j.enconman.2010.06.031.

[13] Conway BE, Birss V, Wojtowicz J. The role and utilization of pseudocapacitance for energy storage by supercapacitors. J Power Sources. 1997;66:1. https://doi.org/10.1016/S0378-7753(96)02474-3.

[14] Stoller MD, Ruoff RS. Best practice methods for determining an electrode material's performance for ultracapacitors. Energ Environ Sci. 2010;3:1294. https://doi.org/10.1039/C0EE00074D.

[15] Burke A. Ultracapacitors: why, how, and where is the technology. J Power Sources. 2000;91:37. https://doi.org/10.1016/S0378-7753(00)00485-7.

[16] Beguin F, Presser V, Balducci A, Frackowiak E. Carbons and electrolytes for advanced supercapacitors. Adv Mater. 2014;26:2219. https://doi.org/10.1016/S0378-7753(00)00485-7.

[17] Liu WJ, Yuan M, Lian JB, Li GC, Li QP, Qiao F, Zhao Y. Embedding partial sulfurization of iron–cobalt oxide nanoparticles into carbon nanofibers as an efficient electrode for the advanced asymmetric supercapacitor. Tungsten. 2023;5(1):118. https://doi.org/10.1007/s42864-022-00157-2.

[18] Chai SS, Zhang WB, Yang JL, Zhang L, Han XW, Theint MM, Ma XJ. CeO_2-clay composites for ultra-long cycle life electrochemical capacitive energy storage application. J Rare Earths. 2023;41(5):728. https://doi.org/10.1016/j.jre.2022.05.020.

[19] Muzaffar A, Ahamed MB, Deshmukh K, Thirumalai J. A review on recent advances in hybrid supercapacitors: design, fabrication and applications. Renew Sust Energ Rev. 2019;101:123. https://doi.org/10.1016/j.rser.2018.10.026.

[20] Pang J, Mendes RG, Bachmatiuk A, Zhao L, Ta HQ, Gemming T, Liu H, Liu Z, Rummeli MH. Applications of 2D MXenes in energy conversion and storage systems. Chem Soc Rev. 2019;48:72. https://doi.org/10.1039/C8CS00324F.

[21] Li QL, JX Cao, Zhang Q. Tuning mechanism of reduced--graphene oxide content on electrochemical performance of MXene/reduced graphene oxide-based supercapacitors. Chin J Rare Met. 2022;46(9):1133. https://doi.org/10.13373/j.cnki.cjrm.XY21040042.

[22] Ghidiu M, Lukatskaya MR, Zhao MQ, Gogotsi Y, Barsoum MW. Conductive two-dimensional titanium carbide "clay" with high volumetric capacitance. Nature. 2014;516:78. https://doi.org/10.1038/nature13970.

[23] Geng X, Zhang Y, Han Y, Li J, Yang L, Benamara M, Chen L, Zhu H. Two-dimensional water-coupled metallic MoS_2 with nanochannels for ultrafast supercapacitors. Nano Lett. 2017;17:1825. https://doi.org/10.1021/acs.nanolett.6b05134.

[24] Liang M, Zhao M, Wang H, Shen J, Song X. Enhanced cycling stability of hierarchical $NiCo_2S_4$@$Ni(OH)_2$@PPy core-shell nanotube arrays for aqueous asymmetric supercapacitors. J Mater Chem A. 2018;6:2482. https://doi.org/10.1039/C7TA10413H.

[25] Shi F, Li L, Wang X, Gu C, Tu J. Metal oxide/hydroxide-based materials for supercapacitors. RSC Adv. 2014;4:41910. https://doi.org/10.1039/C4RA06136E.

[26] Guo W, Yu C, Li S, Wang Z, Yu J, Huang H, Qiu J. Strategies and insights towards the intrinsic capacitive properties of MnO_2 for supercapacitors: challenges and perspectives. Nano Energy. 2019;57:459. https://doi.org/10.1016/j.nanoen.2018.12.015.
[27] Ji X, Cheng S, Yang L, Jiang Y, Jiang ZJ, Yang C, Zhang H, Liu M. Phase transition-induced electrochemical performance enhancement of hierarchical $CoCO_3$/CoO nanostructure for pseudocapacitor electrode. Nano Energy. 2015;11:736. https://doi.org/10.1016/j.nanoen.2014.11.064.
[28] Xiao H, Yao S, Liu H, Qu F, Zhang X, Wu X. NiO nanosheet assembles for supercapacitor electrode materials. Prog Nat Sci. 2016;26:271. https://doi.org/10.1016/j.pnsc.2016.05.007.
[29] Qin B, Wang M, Wu S, Li Y, Liu C, Zhang Y, Fan H. Carbon dots confined nanosheets assembled $NiCo_2S_4$@CDs cross--stacked architecture for enhanced sodium ion storage. Chinese Chem Lett. 2023. https://doi.org/10.1016/j.cclet.2023.108921.
[30] Du M, Guo J, Zheng S, Liu Y, Yang J, Zhang K, Gu Z, Wang X, Wu X. Direct reuse of $LiFePO_4$ cathode materials from spent lithium-ion batteries: extracting Li from brine. Chinese Chem Lett. 2023;34:107706. https://doi.org/10.1016/j.cclet.2022.07.049.
[31] Gu Z, Wang X, Heng Y, Zhang K, Liang H, Yang J, Ang E, Wang P, You Y, Du F, Wu X. Prospects and perspectives on advanced materials for sodium-ion batteries. Sci Bull. 2023;68:2302. https://doi.org/10.1016/j.scib.2023.08.038.
[32] Gu Z, Heng Y, Guo J, Cao J, Wang X, Zhao X, Sun Z, Zheng S, Liang H, Li B, Wu X. Nano self-assembly of fluorophosphate cathode induced by surface energy evolution towards high-rate and stable sodium-ion batteries. Nano Res. 2023;16:439. https://doi.org/10.1007/s12274-022-4687-6.
[33] Kong D, Ren W, Cheng C, Wang Y, Huang Z, Yang HY. Three-dimensional $NiCo_2O_4$@polypyrrole coaxial nanowire arrays on carbon textiles for high-performance flexible asymmetric solid-state supercapacitor. ACS Appl Mater Interfaces. 2015;7:21334. https://doi.org/10.1021/acsami.5b05908.
[34] Natarajan S, Ulaganathan M, Aravindan V. Building next-generation supercapacitors with battery type $Ni(OH)_2$. J Mater Chem A. 2021;9:15542. https://doi.org/10.1039/D1TA03262C.
[35] Xia C, Li P, Gandi AN, Schwingenschlögl U, Alshareef HN. Is $NiCo_2S_4$ really a semiconductor? Chem Mater. 2015;27:6482. https://doi.org/10.1021/acs.chemmater.5b01843.
[36] Pei Y, Cheng Y, Chen J, Smith W, Dong P, Ajayan PM, Ye M, Shen J. Recent developments of transition metal phosphides as catalysts in the energy conversion field. J Mater Chem A. 2018;6:23220. https://doi.org/10.1039/C8TA09454C.
[37] Zong Q, Liu C, Yang H, Zhang Q, Cao G. Tailoring nanostructured transition metal phosphides for high-performance hybrid supercapacitors. Nano Today. 2021;38:101201. https://doi.org/10.1016/j.nantod.2021.101201.
[38] Xie J, Ji Y, Kang J, Sheng J, Mao D, Fu X, Sun R, Wong C. In situ growth of $Cu(OH)_2$@FeOOH nanotube arrays on catalytically deposited Cu current collector patterns for high-performance flexible in-plane micro-sized energy storage devices. Energ Environ Sci. 2019;12:194. https://doi.org/10.1039/C8EE01979G.
[39] Peng S, Li L, Tan H, Cai R, Shi W, Li C, Mhaisalkar SG, Srinivasan M, Ramakrishna S, Yan Q. MS_2(M = Co and Ni) hollow spheres with tunable interiors for high-performance supercapacitors and photovoltaics. Adv Funct Mater. 2014;24:2155–62. https://doi.org/10.1002/adfm.201303273.
[40] Yi M, Xiang F, Yue X, Zhou X, Jiang N, Zheng Q, Lin D. Porous $Ni_2P/Co_2(P_2O_7)$ heterojunction nanosheets as an advanced electrode for high-performance supercapacitors. Appl Surf Sci. 2022;604:154503. https://doi.org/10.1016/j.apsusc.2022.154503.
[41] Delbari SA, Ghadimi LS, Hadi R, Farhoudian S, Nedaei M, Babapoor A, Sabahi Namini A, Le QV, Shokouhimehr M, Asl MS, Mohammadi M. Transition metal oxide-based electrode materials for flexible supercapacitors: A review. J Alloy Compd. 2021;857:158281. https://doi.org/10.1016/j.jallcom.2020.158281.
[42] Hu C, Chang K, Lin M, Wu Y. Design and tailoring of the nanotubular arrayed architecture of hydrous RuO_2 for next generation supercapacitors. Nano Lett. 2006;6:2690. https://doi.org/10.1021/nl061576a.
[43] Nunes WG, Miranda AN, Freitas B, Vicentini R, Oliveira AC, Doubek G, Freitas RG, Da Silva LM, Zanin H. Charge-storage mechanism of highly defective NiO nanostructures on carbon nanofibers in electrochemical supercapacitors. Nanoscale. 2021;13:9590. https://doi.org/10.1039/D1NR00065A.
[44] Yang G, Zhang Z, Zhang Z, Zhang L, Xue Y, Yang J, Peng C. Rational construction of well-defined hollow double shell SnO_2/mesoporous carbon spheres heterostructure for supercapacitors. J Alloy Compound. 2021;873:159810. https://doi.org/10.1016/j.jallcom.2021.159810.
[45] Liu S, Kang L, Hu J, Jung E, Zhang J, Jun SC, Yamauchi Y. Unlocking the potential of oxygen-deficient copper-doped Co_3O_4 nanocrystals confined in carbon as an advanced electrode for flexible solid-state supercapacitors. ACS Energy Lett. 2021;6:3011. https://doi.org/10.1021/acsenergylett.1c01373.
[46] Fu Y, Song J, Zhu Y, Cao C. High-performance supercapacitor electrode based on amorphous mesoporous $Ni(OH)_2$ nanoboxes. J Power Sources. 2014;262:344. https://doi.org/10.1016/j.jpowsour.2014.04.002.
[47] Cao L, Xu F, Liang YY, Li HL. Preparation of the novel nanocomposite $Co(OH)_2$/ultra-stable Y zeolite and its application as a supercapacitor with high energy density. Adv Mater. 2004;16:1853. https://doi.org/10.1002/adma.200400183.
[48] Wu N, Kuo S, Lee M. Preparation and optimization of RuO_2-impregnated SnO_2 xerogel supercapacitor. J Power Sources. 2002;104:62. https://doi.org/10.1016/S0378-7753(01)00873-4.
[49] Zheng J, Cygan PJ, Jow TR. Hydrous ruthenium oxide as an electrode material for electrochemical capacitors. J Electrochem Soc. 1995;142:2600. https://doi.org/10.1149/1.2050077/meta.
[50] Jeon S, Jeong JH, Yoo H, Yu HK, Kim BH, Kim MH. RuO_2 nanorods on electrospun carbon nanofibers for supercapacitors. ACS Appl Nano Mater. 2020;3:3847. https://doi.org/10.1021/acsanm.0c00579.
[51] Li L, Hu Z, An N, Yang Y, Li Z, Wu H. Facile synthesis of MnO_2/CNTs composite for supercapacitor electrodes with long cycle stability. J Phys Chem C. 2014;118:22865. https://doi.org/10.1021/jp505744p.
[52] Cheng S, Yang L, Chen D, Ji X, Jiang Z, Ding D, Liu M. Phase evolution of an alpha MnO_2-based electrode for pseudo-capacitors probed by in operando raman spectroscopy. Nano Energy. 2014;9:161. https://doi.org/10.1016/j.nanoen.2014.07.008.
[53] Xu Z, Sun S, Cui W, Lv J, Geng Y, Li H, Deng J. Interconnected network of ultrafine MnO_2 nanowires on carbon cloth with weed-like morphology for high-performance supercapacitor electrodes. Electrochim Acta. 2018;268:340. https://doi.org/10.1016/j.electacta.2018.02.138.
[54] Hu X, Wei L, Chen R, Wu Q, Li J. Reviews and prospectives of Co_3O_{4-} based nanomaterials for supercapacitor application. ChemistrySelect. 2020;5:5268. https://doi.org/10.1002/slct.201904485.
[55] Xiao Y, Dai A, Zhao X, Wu S, Su D, Wang X, Fang S. A comparative study of one-dimensional and two-dimensional

porous CoO nanomaterials for asymmetric supercapacitor. J Alloy Compd. 2019;781:1006. https://doi.org/10.1016/j.jallcom.2018.12.129.
[56] Li Y, An F, Wu H, Zhu S, Lin C, Xia M, Xue K, Zhang D, Lian K. A $NiCo_2S_4$ /hierarchical porous carbon for high performance asymmetrical supercapacitor. J Power Sources. 2019;427:138. https://doi.org/10.1016/j.jpowsour.2019.04.060.
[57] Bode H, Dehmelt K, Witte J. Zur kenntnis der nickelhydroxidelektrode-I.Über das nickel (II)-hydroxidhydrat. Electrochim Acta. 1966;11:1079. https://doi.org/10.1016/0013-4686(66)80045-2.
[58] Lokhande PE, Pawar P, Chavan US. Chemically deposited ultrathin a-$Ni(OH)_2$ nanosheet using surfactant on Ni foam for high performance supercapacitor application. Mater Sci Energy Technol. 2018. https://doi.org/10.1016/j.mset.2018.07.001.
[59] Km DK, Hong JG, Kweon J, Saeed G, Kim KH, Lee D, Kang MC. Spinel $NiCo_2O_4$ nanowires synthesized on Ni foam as innovative binder-free supercapacitor electrodes. Mater Chem Phys. 2022;291:126718. https://doi.org/10.1016/j.matchemphys.2022.126718.
[60] Azizi S, Seifi M, Moghadam MTT, Askari MB, Varma RS. High-capacity $MnCo_2O_4$/$NiCo_2O_4$ as electrode materials for electrochemical supercapacitors. J Phys Chem Solids. 2023;174:111176. https://doi.org/10.1016/j.jpcs.2022.111176.
[61] Tiwari N, Kadam S, Ingole R, Kulkarni S. Facile hydrothermal synthesis of $ZnFe_2O_4$ nanostructures for high-performance supercapacitor application. Ceram Int. 2022;48:29478. https://doi.org/10.1016/j.ceramint.2022.06.276.
[62] Appiagyei AB, Asiedua-Ahenkorah L, Bathula C, Kim HS, Han SS, Rao KM, Anang DA. Rational design of sucrose--derived graphitic carbon coated $MnMoO_4$ for high performance asymmetric supercapacitor. J Energy Storage. 2023;58:106383. https://doi.org/10.1016/j.est.2022.106383.
[63] Wang Q, Wang X. Regulating the supercapacitor properties of hollow NiCo-LDHs via morphology engineering. J Alloy Compd. 2023;937:168396. https://doi.org/10.1016/j.jallcom.2022.168396.
[64] Kulkarni P, Nataraj SK, Balakrishna RG, Nagaraju DH, Reddy MV. Nanostructured binary and ternary metal sulfides: synthesis methods and their application in energy conversion and storage devices. J Mater Chem A. 2017;5:22040. https://doi.org/10.1039/C7TA07329A.
[65] Wu Z, Zhu Y, Ji X. $NiCo_2O_4$-based materials for electrochemical supercapacitors. J Mater Chem A. 2014;2:14759. https://doi.org/10.1039/C4TA02390K.
[66] Wang Z, Wei G, Du K, Zhao X, Liu X, Wang S, Zhou Y, An C, Zhang J. Ni foam-supported carbon-sheathed $NiMoO_4$ nanowires as integrated electrode for high-performance hybrid supercapacitors. ACS Sustainable Chem Eng. 2017;5:5964. https://doi.org/10.1021/acssuschemeng.7b00758.
[67] Zhu X. Recent advances of transition metal oxides and chalcogenides in pseudo-capacitors and hybrid capacitors: A review of structures, synthetic strategies, and mechanism studies. J Energy Storage. 2022;49:104148. https://doi.org/10.1016/j.est.2022.104148.
[68] Liu R, Zhou A, Zhang X, Mu J, Che H, Wang Y, Wang TT, Zhang Z, Kou Z. Fundamentals, advances and challenges of transition metal compounds-based supercapacitors. Chem Eng J. 2021;412:128611. https://doi.org/10.1016/j.cej.2021.128611.
[69] Pang H, Wei C, Li X, Li G, Ma Y, Li S, Chen J, Zhang J. Microwave-assisted synthesis of NiS_2 nanostructures for supercapacitors and cocatalytic enhancing photocatalytic H_2 production. Sci Rep. 2014;4:1. https://doi.org/10.1038/srep03577.
[70] Wu D, Xie X, Zhang J, Ma Y, Hou C, Sun X, Yang X, Zhang Y, Kimura H, Du W. Embedding NiS nanoflakes in electrospun carbon fibers containing NiS nanoparticles for hybrid supercapacitors. Chem Eng J. 2022;446:137262. https://doi.org/10.1016/j.cej.2022.137262.
[71] Sivanantham A, Ganesan P, Shanmugam S. Hierarchical $NiCo_2S_4$ nanowire arrays supported on Ni foam: an efficient and durable bifunctional electrocatalyst for oxygen and hydrogen evolution reactions. Adv Funct Mater. 2016;26:4661. https://doi.org/10.1002/adfm.201600566.
[72] Li X, Yan W, Guo S, Liu Y, Niu J, Yin L, Wang Z. One-step electrochemical controllable preparation of nickel cobalt sulfide nanosheets and its application in supercapacitors. Electrochim Acta. 2021;387:138488. https://doi.org/10.1016/j.electacta.2021.138488.
[73] Liu L, Li Z, Wang H. Dual regulation strategy to enhance the electrochemical performance of rich sulfur vacancies $NiCo_2S_4$ integrate electrode material for supercapacitors. Electrochim Acta. 2023;441:141819. https://doi.org/10.1016/j.electacta.2023.141819.
[74] Zhu Y, Zong Q, Zhang Q, Yang H, Wang Q, Wang H. Three-dimensional core-shell NiCoP@NiCoP array on carbon cloth for high performance flexible asymmetric supercapacitor. Electrochim Acta. 2019;299:441. https://doi.org/10.1016/j.electacta.2019.01.043.
[75] Lei X, Ge S, Tan Y, Wang Z, Li J, Li X, Hu G, Zhu X, Huang M, Zhu Y, Xiang B. High capacity and energy density of Zn-Ni-Co-P nanowire arrays as an advanced electrode for aqueous asymmetric supercapacitor. ACS Appl Mater Interfaces. 2020;12:9158. https://doi.org/10.1021/acsami.9b17038.
[76] Xie M, Zhou M, Zhang Y, Du C, Chen J, Wan L. Freestanding trimetallic Fe-Co-Ni phosphide nanosheet arrays as an advanced electrode for high-performance asymmetric supercapacitors. J Colloid Interface Sci. 2022;608:79. https://doi.org/10.1016/j.jcis.2021.09.159.
[77] Wang F, Lei H, Peng H, Zhou J, Zhao R, Liang J, Ma G, Lei Z. Interlaced nickel phosphide nanoflakes wrapped orthorhombic niobium pentoxide nanowires array for sustainable aqueous asymmetric supercapacitor. Electrochim Acta. 2019;325:134934. https://doi.org/10.1016/j.electacta.2019.134934.
[78] Zhang Z, Liu S, Xiao J, Wang S. Fiber-based multifunctional nickel phosphide electrodes for flexible energy conversion and storage. J Mater Chem A. 2016;4:9691. https://doi.org/10.1039/C6TA03732A.
[79] Zhou K, Zhou W, Yang L, Lu J, Cheng S, Mai W, Tang Z, Li L, Chen S. Ultrahigh-performance pseudocapacitor electrodes based on transition metal phosphide nanosheets array via phosphorization: a general and effective approach. Adv Funct Mater. 2015;25:7530. https://doi.org/10.1002/adfm.201503662.
[80] Ding R, Li X, Shi W, Xu Q, Liu E. One-pot solvothermal synthesis of ternary Ni-Co-P micro/nano-structured materials for high performance aqueous asymmetric supercapacitors. Chem Eng J. 2017;320:376. https://doi.org/10.1016/j.cej.2017.03.060.
[81] Huang Y, Li M, Chen S, Sun P, Lv X, Li B, Fang L, Sun X. Constructing aqueous Zn//Ni hybrid battery with NiSe nanorod array on nickel foam and redox electrolytes for high-performance electrochemical energy storage. Appl Surf Sci. 2021;562:150222. https://doi.org/10.1016/j.apsusc.2021.150222.
[82] Yu N, Zhu MQ, Chen D. Flexible all-solid-state asymmetric supercapacitors with three-dimensional $CoSe_2$/carbon cloth electrodes. J Mater Chem A. 2015;3:7910. https://doi.org/10.1039/C5TA00725A.
[83] Zhang Y, Pan A, Wang Y, Cao X, Zhou Z, Zhu T, Liang S, Cao G. Self-templated synthesis of N-doped $CoSe_2$/C double-shelled dodecahedra for high-performance supercapacitors. Energy Storage Mater. 2017;8:28. https://doi.org/10.1016/j.ensm.2017.03.005.

[84] Subhadarshini S, Pavitra E, Rama Raju GS, Chodankar NR. Goswami DK, Han YK, Huh YS, Das NC, One-dimensional NiSe-Se hollow nanotubular architecture as a binder-free cathode with enhanced redox reactions for high-performance hybrid supercapacitors. ACS Appl Mater Interfaces. 2020;12: 29302. https://doi.org/10.1021/acsami.0c05612.
[85] Miao C, Zhou C, Wang HE, Zhu K, Ye K, Wang Q, Yan J, Cao D, Li N, Wang G. Hollow Co-Mo-Se nanosheet arrays derived from metal-organic framework for high-performance supercapacitors. J Power Sources. 2021;490:229532. https://doi.org/10.1016/j.jpowsour.2021.229532.
[86] Tavakoli F, Rezaei B, Taghipour Jahromi AR, Ensafi AA. Facile synthesis of yolk-shelled $CuCo_2Se_4$ microspheres as a novel electrode material for supercapacitor application. ACS Appl Mater Interfaces. 2020;12:418. https://doi.org/10.1021/acsami.9b12805.
[87] Yang P, Wu Z, Jiang Y, Pan Z, Tian W, Jiang L, Hu L. Fractal $(Ni_xCo_{1-x})_9Se_8$ nanodendrite arrays with highly exposed (011) surface for wearable, all-solid-state supercapacitor. Adv Energy Mater. 2018;8:1801392. https://doi.org/10.1002/aenm.201801392.
[88] Hosseini H, Shahrokhian S. Self-supported nanoporous Zn-Ni-Co/Cu selenides microball arrays for hybrid energy storage and electrocatalytic water/urea splitting. Chem Eng J. 2019;375:122090. https://doi.org/10.1016/j.cej.2019.122090.
[89] Santhoshkumar P, Nagaraju G, Shaji N, Sim GS, Nanthagopal M, Sekhar SC, Yu JS, Lee CW. Hierarchical iron selenide nanoarchitecture as an advanced anode material for high-performance energy storage devices. Electrochim Acta. 2020;356: 136833. https://doi.org/10.1016/j.electacta.2020.136833.
[90] Yang X, Zhang J, Wang Z, Wang H, Zhi C, Yu DYM, Rogach AL. Carbon-supported nickel selenide hollow nanowires as advanced anode materials for sodium-ion batteries. Small. 2018;14:1702669. https://doi.org/10.1002/smll.201702669.
[91] Shi X, Wang H, Kannan P, Ding J, Ji S, Liu F, Gai H, Wang R. Rich-grain-boundary of Ni_3Se_2 nanowire arrays as multifunctional electrode for electrochemical energy storage and conversion applications. J Mater Chem A. 2019;7:3344. https://doi.org/10.1039/C8TA10912E.
[92] Zhao L, Zhang P, Zhang Y, Zhang Z, Yang L, Chen ZG. Facile synthesis of hierarchical Ni_3Se_2 nanodendrite arrays for supercapacitors. J Mater Sci Technol. 2020;54:69. https://doi.org/10.1016/j.jpowsour.2013.12.030.
[93] Qu G, Zhang X, Xiang G, Wei Y, Yin J, Wang Z, Zhang X, Xu X. ZIF-67 derived hollow Ni-Co-Se nano-polyhedrons for flexible hybrid supercapacitors with remarkable electrochemical performances. Chinese Chem Lett. 2020;31:2007. https://doi.org/10.1016/j.cclet.2020.01.040.
[94] Zhang Y, Hu Z, Liang Y, Yang Y, An N, Li Z, Wu H. Growth of 3D SnO_2 nanosheets on carbon cloth as a binder-free electrode for supercapacitors. J Mater Chem A. 2015;3:15057. https://doi.org/10.1039/C5TA02479J.
[95] Xu Z, Li X, Sun S, Wang X, Zhang Z, Li H, Yin S. High mass loading NiCoAl layered double hydroxides with interlayer spacing and interface regulation for high-capacity and long-life supercapacitors. J Power Sources. 2022;546:231982. https://doi.org/10.1016/j.jpowsour.2022.231982.
[96] Xu Z, Li X, Sun S, Wei Z, Li H, Yin S. Multidimensional carbon-modified $NiCo_2O_4$/Ni-Co-S nanocomposite electrode material for high-energy asymmetric supercapacitors. Energy Fuels. 2021;35:9692. https://doi.org/10.1021/acs.energyfuels.1c01075.
[97] Cheng Y. Fabrication of sugar-coated $CoNi_2S_4/Ni_3P$ nanostructure with ultrahigh electrochemical performance for supercapacitor application. Int J Electrochem Sci. 2021;16: 210440. https://doi.org/10.20964/2021.04.48.
[98] Wei TY, Chen CH, Chang KH, Lu SY, Hu CC. Cobalt oxide aerogels of ideal supercapacitive properties prepared with an epoxide synthetic route. Chem Mater. 2009;21:3228. https://doi.org/10.1021/cm9007365.
[99] Younas W, Naveed M, Cao C, Khalid S, Rafai S, Wang Z, Wu Y, Yang L. Rapid and simplistic microwave assisted method to synthesise cobalt selenide nanosheets; a prospective material for high performance hybrid supercapacitor. Appl Surf Sci. 2020; 505:144618. https://doi.org/10.1016/j.apsusc.2019.144618.
[100] Patil SJ, Bulakhe RN, Lokhande CD. Nanoflake-modulated La_2Se_3 thin films prepared for an asymmetric supercapacitor device. ChemPlusChem. 2015;80:1478. https://doi.org/10.1002/cplu.201500009.
[101] Chen H, Jiang J, Zhang L, Xia D, Zhao T, Guo D, Qi T, Wan H. In situ growth of $NiCo_2S_4$ nanotube arrays on Ni foam for supercapacitors: maximizing utilization efficiency at high mass loading to achieve ultrahigh areal pseudocapacitance. J Power Sources. 2014;254:249. https://doi.org/10.1016/j.jpowsour.2013.12.092.
[102] Banerjee A, Bhatnagar S, Upadhyay KK, Yadav P, Ogale S. Hollow $Co_{0.85}Se$ nanowire array on carbon fiber paper for high rate pseudocapacitor. ACS Appl Mater Interfaces. 2014;6: 18844. https://doi.org/10.1021/am504333z.
[103] Peng H, Zhou J, Sun K, Ma G, Zhang Z, Feng E, Lei Z. High-performance asymmetric supercapacitor designed with a novel NiSe@$MoSe_2$ nanosheet array and nitrogen-doped carbon nanosheet. ACS Sustainable Chem Eng. 2017;5:5951. https://doi.org/10.1021/acssuschemeng.7b00729.
[104] Wu Z, Zhong Y, Liu J, Wu J, Guo X, Zhong B, Zhang Z. Subunits controlled synthesis of α-Fe_2O_3 multi-shelled core--shell microspheres and their effects on lithium/sodium ion battery performances. J Mater Chem A. 2015;3:10092. https://doi.org/10.1039/C5TA01334H.
[105] Huang L, Waller GH, Ding Y, Chen D, Ding D, Xi P, Wang ZL, Liu M. Controllable interior structure of $ZnCo_2O_4$ microspheres for high-performance lithium-ion batteries. Nano Energy. 2015; 11:64. https://doi.org/10.1016/j.nanoen.2014.09.027.
[106] Wang X, Feng J, Bai Y, Zhang Q, Yin Y. Synthesis, properties, and applications of hollow micro-/nanostructures. Chem Rev. 2016;116:10983. https://doi.org/10.1021/acs.chemrev.5b00731.
[107] Wang X, Sun P, Qin J, Wang J, Xiao Y, Cao M. A three-dimensional porous MoP@C hybrid as a high-capacity, long-cycle life anode material for lithium-ion batteries. Nanoscale. 2016;8: 10330. https://doi.org/10.1039/C6NR01774F.
[108] Rauf M, Shah SS, Shah SK, Shah SNA, Haq TU, Shah J, Ullah A, Ahmad T, Khan Y, Aziz MA, Hayat K. Facile hydrothermal synthesis of zinc sulfide nanowires for high-performance asymmetric supercapacitor. J Saudi Chem Soc. 2022;26: 101514. https://doi.org/10.1016/j.jscs.2022.101514.
[109] Zaulkiflee ND, Ahmad AL, Low SC, Norikazu N. Recent advances on the utilization of nanosheets as electrode material for supercapacitor application. J Energy Storage. 2022;55: 105697. https://doi.org/10.1016/j.est.2022.105697.
[110] Liu Q, Ding Y, Zhang L, Li Y, Jiang C, Cheng L, Li Z. Self-supported electrode constructed by hierarchical nickel-cobalt selenide nanosheet arrays for high-performance flexible supercapacitors. Colloid Surface A. 2023;661:130934. https://doi.org/10.1016/j.colsurfa.2023.130934.
[111] Han Y, Sun S, Cui W, Deng J. Multidimensional structure of $CoNi_2S_4$ materials: structural regulation promoted electrochemical performance in a supercapacitor. RSC Adv. 2020;10: 7541. https://doi.org/10.1039/C9RA10961G.
[112] Cao Y, Li W, Xu K, Zhang Y, Ji T, Zou R, Yang J, Qin Z, Hu J. $MnMoO_4{\cdot}4H_2O$ nanoplates grown on a Ni foam substrate for excellent electrochemical properties. J Mater Chem A. 2014;2: 20723. https://doi.org/10.1039/C4TA04019H.

[113] Zhang Z, Zhang H, Zhang X, Yu D, Ji Y, Sun Q, Wang Y, Liu X. Facile synthesis of hierarchical $CoMoO_4$@$NiMoO_4$ core--shell nanosheet arrays on nickel foam as an advanced electrode for asymmetric supercapacitors. J Mater Chem A. 2016;4:18578. https://doi.org/10.1039/C6TA06848K.
[114] Adhikari S, Noh GH, Kim DH. Core-shell 2D/2D $FeCo_2O_4$@$Ni(OH)_2$ nano-on-microsheet array architecture for excellent asymmetric supercapacitor performance. Appl Surf Sci. 2023;611:155449. https://doi.org/10.1016/j.apsusc.2022.155449.
[115] Sun W, Lu Q. Self-supported α-$Ni(OH)_2$ nanosheet arrays modified with carbon quantum dots for high-performance supercapacitors. Scripta Mater. 2023;224:115119. https://doi.org/10.1016/j.scriptamat.2022.115119.
[116] Yuan Y, Wang W, Yang J, Tang H, Ye Z, Zeng Y, Lu J. Three-Dimensional $NiCo_2O_4$@$MnMoO_4$ core-shell nanoarrays for high-performance asymmetric supercapacitors. Langmuir. 2017;33:10446. https://doi.org/10.1021/acs.langmuir.7b01966.